Separation and Purification Technology 340 (2024) 126747

Contents lists available at ScienceDirect

Separation and Purification Technology

journal homepage: www.elsevier.com/locate/seppur

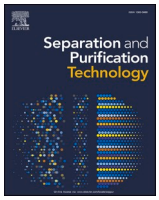

Upcycled PVC support layer from waste PVC pipe for thin film composite nanofiltration membranes

Atta Ur Razzaq, Milad Rabbani Esfahani *

Department of Chemical and Biological Engineering, The University of Alabama, Tuscaloosa 35487, United States

ARTICLE INFO

Editor: V. Tarabara

Keywords:
Plastic pollution
Plastic upcycling
Filtration
Clean environment
Wastewater treatment

ABSTRACT

Thin-film-composite (TFC) nanofiltration membranes represent the pinnacle of membrane technology in water treatment and desalination. These membranes typically consist of a polyamide (PA) selective layer and a membrane support layer, often constructed from commercially available materials like polyethersulfone (PES). However, there exists an alternative approach that involves the use of different polymers, preferably upcycled waste polymers, as a viable support layer for TFC membranes. Successfully implementing the upcycling of waste plastics into high-value support membranes can make a significant contribution to addressing the issue of plastic waste pollution. One of the primary challenges associated with utilizing upcycled polymers as support layers is the potential impact on the polyamide selective layer of TFC membranes, subsequently affecting their performance in terms of permeability, rejection, and antifouling properties. In this study, we demonstrate the successful fabrication of TFC membranes with a support layer crafted from upcycled waste PVC pipe. We conducted a comprehensive investigation into the effects of upcycled PVC on the structural and physicochemical properties of the polyamide layer. The ultrafiltration (UF) support membranes were fabricated from waste PVC pipe via the nonsolvent induced phase separation (NIPS) method. Subsequently, a polyamide layer was synthesized atop the Upcycled PVC membrane using interfacial polymerization (IP). The physicochemical properties and performance of the TFC membranes with upcycled PVC support layer were compared with membranes with research-grade (RG) PVC and commercial PES support layers. The results unveiled that the TFC membrane with upcycled PVC support layer exhibited higher water permeability (18.2 LMH/bar), in contrast to RG TFC (15.5 LMH/bar) and PES TFC membranes (13.7 LMH/bar). Furthermore, the salt rejection capabilities of the upcycled PVC TFC membrane were competitive and well within an acceptable range.

1. Introduction

Plastic production has increased 20 times over the past 50 years, with an estimated 9200 million metric tons (Mt) of plastic produced worldwide, of which more than 6900 Mt end up in landfills and lead to environmental pollution. 368 Mt of plastics were produced globally in 2019, which is expected to double within the next 20 years [1]. This also results in the generation of large quantities of plastic waste and widespread plastic pollution. It is estimated that 19–23 Mt of plastic waste produced worldwide in 2016 entered into the aquatic bodies and is estimated to rise up to 53 Mt annually by 2030 [1]. Two serious problems involving plastic fragments affecting marine organisms in aquatic ecosystems are entanglement and ingestion which lead to loss of mobility, loss of sensitivity, weakening of reproduction ability, decreased growth and even death [2]. These plastics enter the human body through the food chain, as marine and terrestrial organisms are consumed by humans. They can lead to various health issues, including tissue damage, reproductive problems, mental health issues, intestinal damage, immune system problems, and neurotoxicity [3]. Polyvinyl chloride (PVC) is among the most widely manufactured and utilized thermoplastics globally. It is employed in an array of applications, including pipes, packaging, wire insulation, furniture, automotive components, construction materials, flooring, window frames, and numerous other products [4].

In 2018, the global demand for PVC stood at approximately 44.3 million tons, and it is projected to rise significantly to around 60 million tons by 2025 [5]. This increasing demand for PVC has consequently resulted in a surge in PVC waste production, posing environmental concerns due to the chlorine content, adipate, phthalate, etc. in PVC materials [5]. Notably, a substantial portion of PVC is utilized in the

* Corresponding author.
E-mail address: mesfahani@eng.ua.edu (M.R. Esfahani).

https://doi.org/10.1016/j.seppur.2024.126747
Received 27 November 2023; Received in revised form 26 January 2024; Accepted 7 February 2024
Available online 13 February 2024

production of PVC pipes and fittings, leading to a significant volume of PVC pipe waste generation [6].

Recycling PVC presents a significant challenge due to its high chlorine content. The incineration of PVC leads to the production of toxic chlorinated dioxins and corrosive hydrogen chloride (HCl) gas, posing risks to human health [7]. Landfilling PVC waste is also an unsuitable option because natural exposure can result in oxidative degradation, causing slow decomposition and the release of additives such as phthalates. This can lead to groundwater contamination [7]. Therefore, a more promising solution to address PVC pollution is through upcycling of waste PVC, which involves converting plastic waste into high-value-added products such as polymeric membranes [8].

Presently, thin film composite (TFC) membranes are the predominant choice for large-scale industrial water treatment and desalination applications [9]. These TFC nanofiltration (NF) membranes consist of two key components: a support layer, responsible for providing structural integrity, and a selective polyamide layer, responsible for the separation capabilities of the TFC membrane [10].

Currently, the majority of commercial TFC membranes utilize polyether sulfone (PES) or polysulfone (PSF) as their support layers. However, there is a wealth of research reporting the development of TFC membranes using various porous support materials [11]. While various polymers, including polyethylenepolyethylene (PE) [12], polypropylene (PP) [13], polyimide (PI) [14], polyvinylidene fluoride (PVDF) [15], polyacrilonitrile (PAN) [16], polyphenylsulfone (PPSU), polytetrafluoroethylene (PTFE), polyetherimide (PEI), poly(ether ether ketone) (PEEK), copoly(phthalazinone biphenyl ether sulfone) (PPBES), poly (arylene ether nitrile ketone) (PENK), polyether polyurethane (PF), poly (phthalazinone ether nitrile ketone) (PPENK), and polyketone (PK) [11,17], have been employed to fabricate support layers in TFC membranes, but the upcycling of waste plastics/polymer such as PVC for use as a support layer in TFC membranes remains relatively unexplored.

The interfacial polymerization (IP) reaction, which forms a thin polyamide layer occurs on the surface of the porous support layer; therefore, the properties of the support layer such as its chemistry, surface topography, roughness, porosity, pore size, surface hydrophilicity/hydrophobicity, morphology and surface charge significantly influence the characteristics such as morphology, thickness and transport properties of the resulting polyamide layer which in turn affect the performance such as water permeability and salt rejection of the TFC membranes [11,18]. Furthermore, the addition/presence of additives in the support layer also changes one or all of the aforementioned support layer properties that, in-turn, impact the properties of the resulting polyamide layer and the performance of the TFC membrane [11]. Several studies have reported the impact of different support layer properties on the characteristics and properties of the polyamide layer and the performance of the TFC membranes. Mokarizadeh et al [11], conducted an comprehensive review focusing on the relationship between the support layer, the PA selective layer, and the effect of support layer properties and additives on the physicochemical properties of the PA layer and, consequently, the performance of TFC membranes.

This paper explored the upcycling of waste PVC pipe as a support layer for creating a TFC membrane. The waste PVC pipe, sourced directly from a landfill, transformed into a support layer using the nonsolvent induced phase separation (NIPS) process. Subsequently, a thin polyamide layer was fabricated atop the support layer through interfacial polymerization (IP), resulting in the development of an Upcycled PVC TFC membrane. To assess the impact of additives, present in the waste PVC pipe on various aspects of the upcycled membrane, including the structure, morphology, thickness, transport properties, and performance (water permeability and salt rejection) of the polyamide layer, TFC membranes using commercial research-grade PVC (RG PVC) powder, were fabricated employing identical conditions as those for the fabrication of the Upcycled PVC TFC membrane. Finally, a comparative analysis assessed the physicochemical properties and performance of the Upcycled PVC TFC membrane against the TFC membranes with commercial polyethersulfone (PES) support.

2. Materials and methods

2.1. Materials

Waste PVC pipe was directly collected from a landfill, and its molecular weight was measured using gel permeation chromatography (Table S1). Research-grade (RG) PVC powder (with a molecular weight of approximately 50,000 g/mol and number-average molecular weight of about 35,000 g/mol) was procured from Sigma Aldrich (St. Louis, MO, United States). Commercial polyethersulfone (PES) membranes were obtained from Synder Filtration (Vacaville, CA, United States). High-purity Tetrahydrofuran (THF) (with a purity of ≥99.9 %) was purchased from Honeywell-Burdick & Jackson (Muskegon, MI, United States). N,N-dimethylformamide (DMF) (with a purity of ≥99.9 %) was sourced from VWR Chemicals BDH (Randor, PA, United States). Piperazine (C4H10N2), anhydrous and 99 % pure, was acquired from Bean-Town Chemical (Hudson, NH, United States). 1,3,5-Benzenetricarbonyl trichloride (C6H3(COCl)3) (TMC) was obtained from Tokyo Chemical Industry (TCI) (Portland, Oregon, United States). n-Hexane (CH3(CH2)4CH3) with a purity of 95 % was supplied by J.T.Baker (Phillipsburg, NY, United States). Sodium chloride (NaCl) with a purity of ≥99 % (and a molecular weight of 58.44 g/mol), calcium chloride (CaCl2) anhydrous (with a molecular weight of 110.98 g/mol), and magnesium sulfate (MgSO4) anhydrous (with a molecular weight of 120.36 g/mol) were all purchased from VWR Life Science (Solon, OH, United States). Nitric acid (HNO3) with a purity of 68–70 % was procured from VWR Chemicals BDH (Randor, PA, United States). Pellets of sodium hydroxide (NaOH) with a molecular weight of 40.00 g/mol and a purity of 98.5 % were sourced from Acros Organics (Geel, AN, Belgium). Silver nitrate ($AgNO_3$) with a molecular weight of 169.87 g/mol was obtained from VWR Life Science (Solon, OH, United States), and a silver standard for ICP was purchased from Inorganic Ventures (Christiansburg, VA, United States). Bis(2-ethylhexyl) adipate, having a purity of 99 % and molecular weight of 370.57 g/mol was purchased from Thermo Scientific (Waltham, Massachusetts, United States). Diisononyl Phthalate with a molecular weight of 418.62 g/mol was obtained from Tokyo Chemical Industry (TCI) (Portland, Oregon, United States). Acetone (purity ≥ 99.5 %) was obtained from VWR Chemicals BDH (Randor, PA, United States). Ultra-pure deionized (DI) water from MilliQ was utilized for all experiments.

2.2. Sample pretreatment.

The waste PVC pipes collected from landfill were water-washed and then soaked in acetone to facilitate the cutting process. After softening, the pipes were cut into small pieces with average dimensions of approximately L: 1.19 cm, W: 0.94 cm, and H: 0.386 cm. Following this, the samples were air-dried at room temperature for a duration of one week to ensure complete evaporation of the acetone. The dried pieces were then subjected to a thorough washing with deionized (DI) water and allowed to dry again at room temperature.

2.3. Support membrane fabrication via nonsolvent induced phase separation (NIPS)

Two different dope solutions were prepared by dissolving 22 wt% of each waste PVC pipe and research-grade (RG) PVC in THF and DMF in a volume ratio of 2 to 3, respectively. All the dope solutions were prepared by stirring at 400 rpm at 23 °C for 19 h. The dope solutions were degassed for 4 h before the phase inversion process. The doctor blade was adjusted to a thickness of 150 μm and positioned on a clean glass slide supported by a solid surface. Approximately 20 % of the casting solution was carefully poured within the doctor blade's designated area. The doctor blade, along with the solution, was then smoothly moved

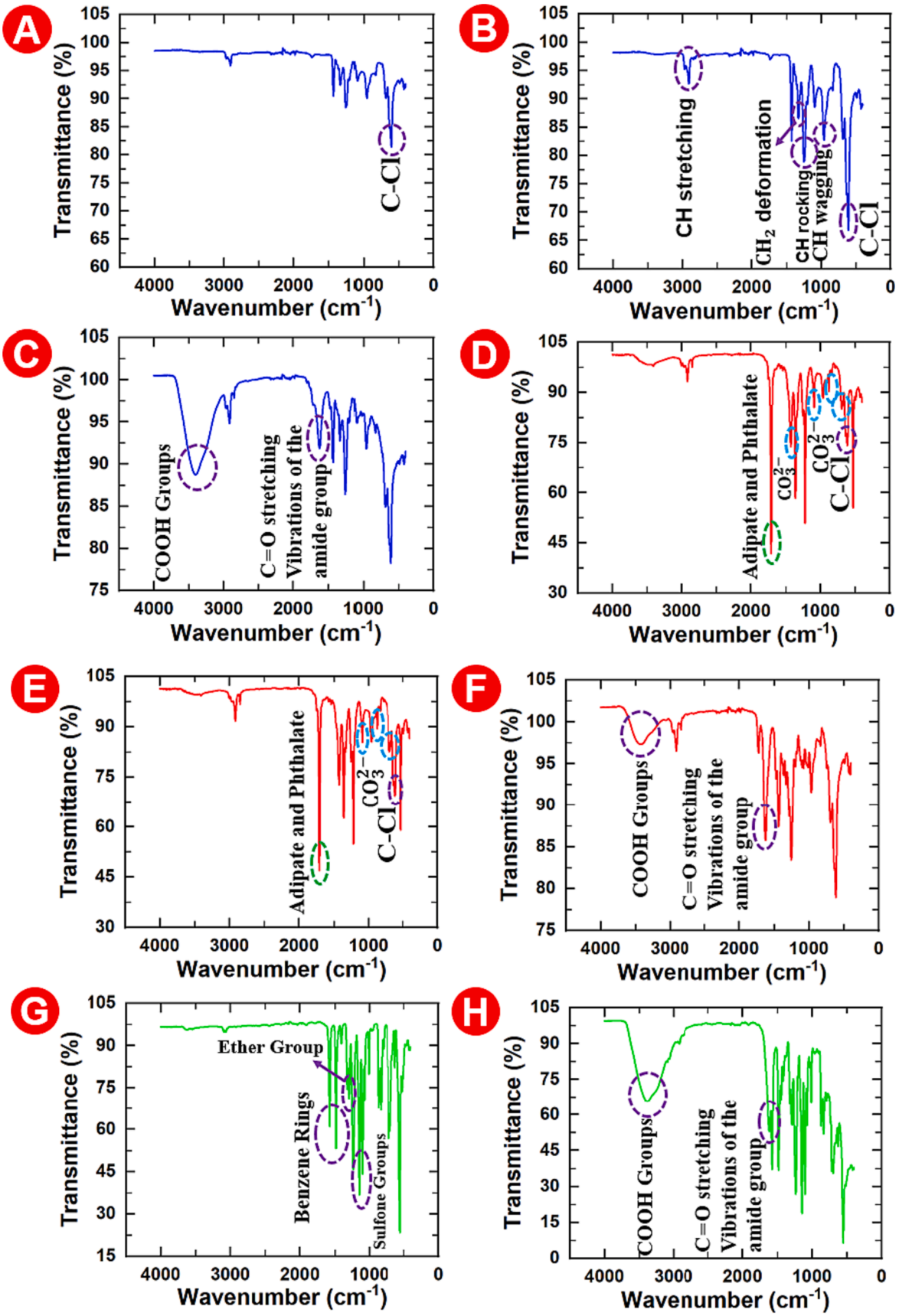

Fig. 1. FTIR of (a) RG PVC powder, (b) RG PVC membrane, (c) RG PVC TFC membrane, (d) PVC pipe piece, (e) Upcycled PVC membrane, (f) Upcycled PVC TFC membrane, (g) PES commercial membrane and (h) PES TFC membrane.

across the glass plate. Subsequently, the solution was allowed to sit undisturbed for one minute. The resulting uniformly flat solution was transferred into a 2 L container of deionized (DI) water, initiating solvent/nonsolvent exchange and causing the membrane to detach from the glass surface. The newly fabricated membrane was gently lifted from the glass plate and stored in refrigerated DI water. The membrane casting was performed at a room temperature of 25 ℃ and an average humidity of 74 %.

2.4. Fabrication of thin film composite (TFC) membranes.

The TFC membranes were prepared by forming a thin polyamide layer on top of the support membranes through interfacial polymerization between piperazine ($C_4H_{10}N_2$) (aqueous phase) and 1,3,5-Benzenetricarbonyl trichloride ($C_6H_3(COCl)_3$) (TMC) (organic phase). The aqueous phase was prepared by dissolving 1 g of piperazine in 99 g of water (1 wt% aqueous piperazine solution) and stirring for 1 h at room temperature. The organic phase was prepared by dissolving 0.15 g of TMC in 100 mL of n-hexane (0.15 wt% of TMC in hexane) and stirring for 1 h at room temperature. The support membranes were taped onto a glass plate and aqueous solution was poured on the membrane surface for 90 s, after which the excess piperazine solution was removed, and the membrane was air knifed for 15 s to completely remove the piperazine from its surface. Following this, the support membrane was immersed in an organic solution containing 0.15 wt% TMC in n-Hexane for 30 s, resulting in the formation of a thin polyamide layer on top of the support membrane. The fabricated TFC membrane was taken out of the organic solution, rinsed three times with DI water, air dried for 2 min, and stored in DI water [19].

2.5. Permeability and salt rejections of the support and TFC membranes.

The permeability of the support and TFC membranes was measured using a cross-flow setup. The membranes were compacted at 120 psi for 2 h to reach a semi-steady-state permeability. This was followed by permeability measurements at 100 psi based on standard protocol (see supporting information S2). The salt rejection of the TFC membranes was measured by passing 2000 ppm aqueous solutions of three salts, sodium chloride (NaCl), calcium chloride ($CaCl_2$), and magnesium sulfate ($MgSO_4$) through the membrane in the cross-flow cell at 100 psi (see supporting information S2).

2.6. Investigate the effect of adipate and phthalate on PA formation

To assess the potential impact of adipate and phthalate, the two primary additives found in PVC pipe, on piperazine diffusion, the same interfacial polymerization (IP) process was conducted. However, this time, only the pure organic phase (n-hexane) was employed instead of a mixture of TMC in hexane. Various amounts of adipate and phthalate (ranging from 0 to 2 wt%) were individually added to the aqueous phase solutions containing 1 wt% piperazine. These solutions were stirred for 30 min. Subsequently, 20 mL of the aqueous phase solution for each condition was poured over RG PVC support membranes for a duration of 90 s. Afterward, the excess aqueous phase was removed, and 20 mL of n-hexane solution was applied to the surface of the RG PVC support membrane for 30 s. During this period, piperazine diffused from the membrane pores into the n-hexane solution. The resulting piperazine-hexane solution was collected in small beakers and allowed to dry overnight, leaving piperazine behind. Once all the hexane had evaporated, piperazine remained in the beakers. To these beakers, 40 mL of water and 0.8 mL of an internal standard (methyl piperazine) were added, and the solutions were stirred for 30 min. The concentration of piperazine was determined using a Bruker HCTUltra PTM Discovery system quadrupole ion trap mass spectrometer in conjunction with an Agilent 1200 capillary LC.

2.7. Characterization techniques.

The surface morphology of the ultrafiltration (UF) support layer and TFC membranes was determined using scanning electron microscopy (SEM, JEOL FE 7000, JEOL, Tokyo, Japan) with gold-coated samples. Fourier transform infrared (FTIR) (Perkinelmer, Waltham, Massachusetts, USA) was used to determine the chemical bonds and functional groups in the membranes. The water contact angle (WCA) of the membranes was determined using the Bio Scientific Attention Theta Lite instrument (Avondale, Arizona, USA). The molecular weight cutoff (MWCO) of the support membranes was measured using polyethylene glycol (PEG) with molecular weights 400, 600, 1000, 1500 and 2000 Da (see supporting information S3) [20]. Ternary phase diagrams for both the PVC pipe and RG PVC casting solutions were established based on the experimental cloud point data obtained through the titration method (see supporting information S4) [21]. Silver binding and elution method was used to measure the carboxylic group density (crosslinking degree) of the polyamide layer (see supporting information S5). The surface charge of the membranes was measured using Surpass 3 (Anton Paar, Houston, Texas, USA). The concentration of the eluted silver ions (Ag^+) was measured using Inductively Coupled Plasma Optical Emission spectroscopy (ICP-OES) (Optima 8300, PerkinElmer, Waltham, United States). The solution conductivity was measured using a conductivity meter (Orion Star A212, Thermo Fisher Scientific, Waltham, United States). The surface roughness of the TFC membranes was measured using atomic force microscopy (AFM) (Innova Scanning Probe Microscope, Bruker, USA). The concentration of piperazine was measured using Bruker HCTUltra PTM Discovery system quadrupole ion trap mass spectrometer coupled with an Agilent 1200 capillary LC and membrane thickness was measured using a micrometer.

3. Results and discussion

3.1. Characterization of Upcycled PVC membrane (support layer)

The thickness measurement of the three support layers—Upcycled PVC, RG PVC, and PES—was performed at ten different points of an individual membrane sheet. The thickness of the commercial PES support membrane with the nonwomen was around 193 ± 0.79 μm and the Upcycled PVC and RG PVC membranes showed a thickness of 184 ± 6.98 and 190 ± 5.23 μm respectively, which were in the same range and, therefore their thickness should not have had any effect on the formation of PA layer (see supporting information S6).

The addition or presence of additives in the support layer changes/alters the properties of the support layer (surface functional groups, hydrophilicity, surface charge, morphology etc.), which impact/alter the piperazine and TMC transport and reaction, hence impacting the thickness, crosslinking degree and morphology of the polyamide layer [15]. The surface chemistry of the support layer impacts the formation and properties of PA selective layer [11]. For instance, a more hydrophilic support has attractive interactions with the aqueous phase which facilitates and improves the penetration of aqueous solution into the support layer and resists the transfer (slows down the diffusion) of aqueous solution to the reaction zone, resulting in the formation of a less crosslinked and thinner PA layer [11,22]. Considering that the PVC pipe incorporates various additives such as adipate and phthalates, a comprehensive FTIR analysis was performed on the Upcycled PVC membranes. The aim was to compare the FTIR results of Upcycled membranes with RG PVC membranes in order to ascertain whether any additives were leached out during the solvation and phase inversion processes. Additionally, a comparative FTIR analysis was conducted on the PA selective layers formed on the surfaces of both Upcycled PVC membranes and RG PVC membranes, as well as commercial PES membranes. This was done to assess the potential alterations in the composition of the PA selective layer. Fig. 1 a and b show the FTIR spectra of RG PVC powder and the RG PVC support membrane, respectively. The

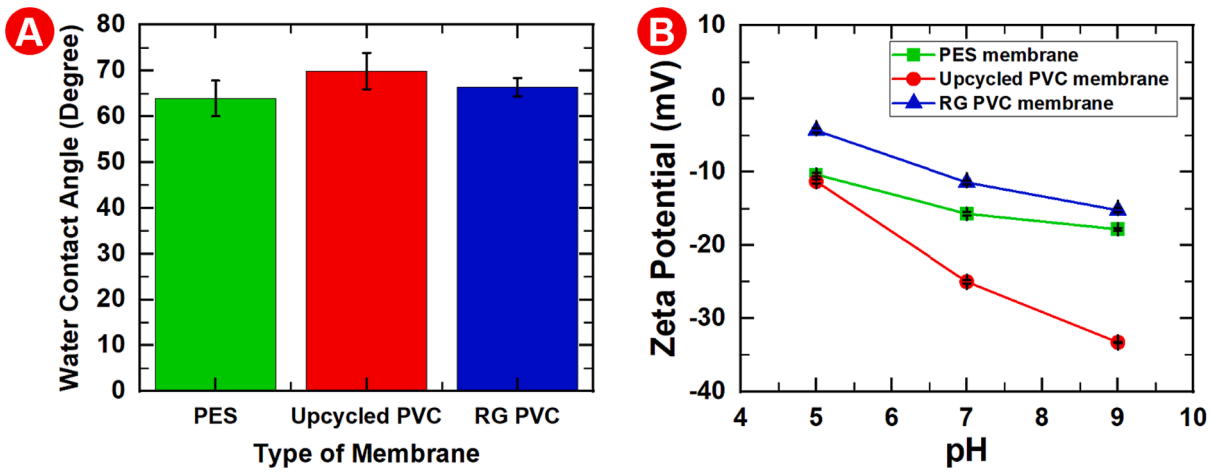

Fig. 2. (a) The water contact angle and (b) The zeta potential (surface charge) of PES, Upcycled PVC, and RG PVC membranes.

FTIR peaks observed in the RG PVC polymer and the RG PVC membrane were found to be identical, providing confirmation that any constituents present in the RG PVC polymer were also retained in the RG PVC support membrane. The PVC peaks include C-Cl bond at 600–650 cm^{-1}, Trans-CH wagging at 961 cm^{-1}, CH rocking at 1240–1257 cm^{-1}, CH_2 deformation at 1339 cm^{-1} and C–H stretching at 2890–2958 cm^{-1} [23,24]. Fig. 1 d and e display the FTIR spectra of the solid PVC pipe and Upcycled PVC membrane, respectively. The FTIR spectra of the PVC pipe and Upcycled PVC exhibit identical peaks, confirming the presence of all components, including various additives, from the waste PVC pipe in the Upcycled PVC. The three main additives of PVC pipe are calcium carbonate, adipate and phthalate [25–27]. The carbonate peaks were identified by in-plane bending of carbonate ion at 700 cm^{-1}, out of plane bending adsorption of carbonate ion at 870 cm^{-1}, the symmetric stretch of carbonate ion at 1080 $cm^{-1,}$ and the asymmetric stretch of carbonate ion at 1400 cm^{-1} [28]. The adipate was identified by the peak at 1700 $cm^{-1,}$ which represents the stretching vibration of C=O group in adipate [29], and phthalate peaks were identified by the symmetric and asymmetric stretching vibrations of the saturated C–H at 2872, 2934 and 2967 cm^{-1}, the stretching vibration of C=O at 1700/1730, the C–C stretching vibration peaks of the benzene ring at 1575 cm^{-1} and 1599 cm^{-1}, The symmetric and asymmetric stretching vibrations of the $–CH_3$ group at 1465 and 1385 cm^{-1} and the ortho- substituted benzene stretching vibrations at 745 cm^{-1} [30]. Fig. 1g shows FTIR of commercial PES support membrane with characteristic peaks of benzene rings at 1576 cm^{-1}, 1483.7 cm^{-1}, and 1405 cm^{-1}, ether function at 1319 cm^{-1}, as well as 1296 cm^{-1} and sulfone group at 1144 cm^{-1} and 1100 cm^{-1} [31]. The FTIR of all the TFC membranes confirmed the formation of PA layer on three support layers (Fig. 1 c, f, and h). A strong broad band at 1627 cm^{-1}, corresponds to the C=O stretching vibrations of the amide group. The peak at about 3399–3440 cm^{-1} which corresponds to –COOH functional groups in poly (piperazine-amide) indicates the carboxylic acid functional groups formed by the partial hydrolysis of the acyl chloride of TMC [10,32]. The comparative analysis of the FTIR spectra of the PA layers formed on the three support layers revealed no discernible alterations in the chemical composition of the PA. This outcome confirmed that the additives present in the Upcycled PVC membrane exerted no influence on the chemical structure of the PA layer.

The water contact angle, which reflects the hydrophilicity/hydrophobicity of the surface of the three membranes (support layer) is presented in Fig. 2a. In general, hydrophilic supports tend to enhance the wettability of the aqueous solution containing amine monomers. Consequently, this elevated wettability contributes to impeding or decelerating the diffusion of amine monomers toward the organic-aqueous interface—the site where the reaction occurs. This hindrance arises due to interactions transpiring between the aqueous phase (comprising water and amine monomers) and the pore walls of the

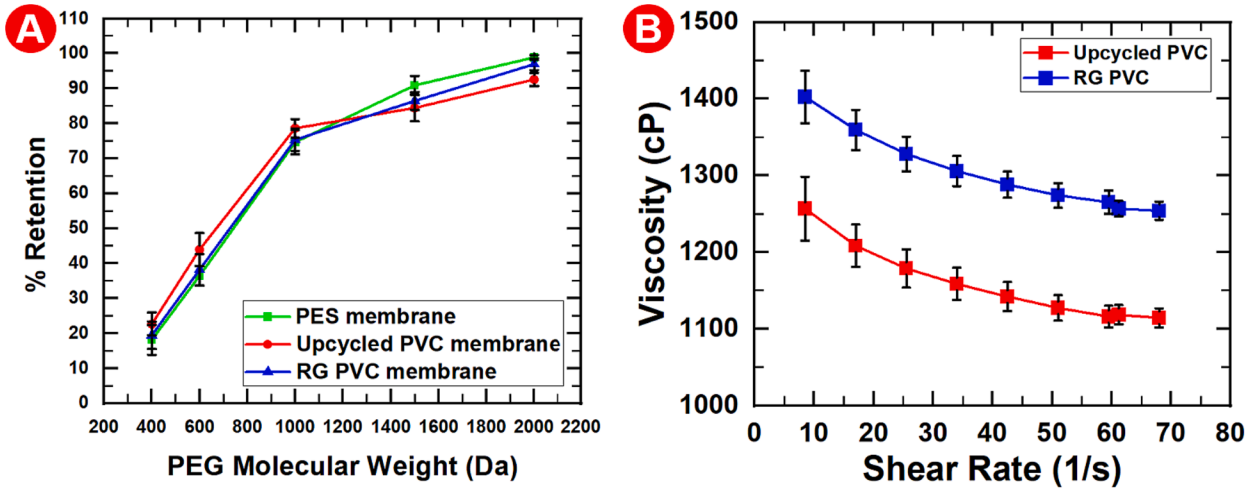

Fig. 3. (a) Molecular Weight Cutoff (MWCO) of PES, Upcycled PVC and RG PVC support membranes measured using different PEG at pressure of 60 psi, (b) Viscosity of PVC Pipe and RG PVC casting solutions at different shear rates measured at the ambient temperature of 23 °C. The concentration of the casting solutions was 22 wt % in a mixture of DMF:THF (v/v) 3:2, stirred at 400 rpm for 19 h at 23 °C.

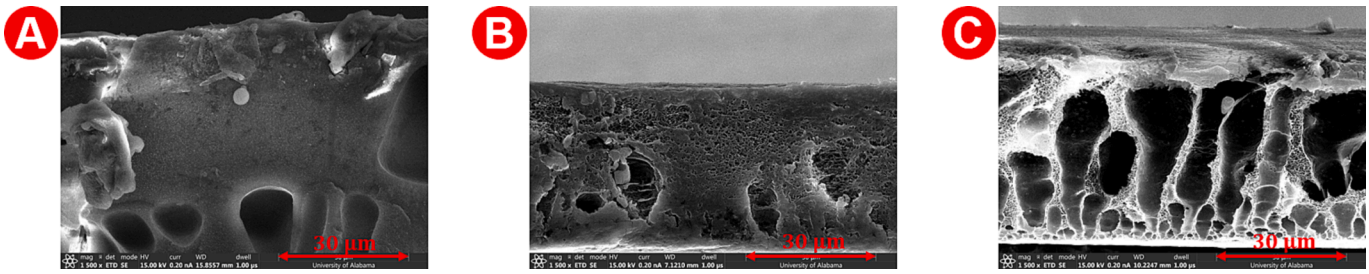

Fig. 4. SEM cross-section of (a) PES, (b) RG PVC and (c) Upcycled PVC membranes. Prior to SEM, the samples were gold sputtered at 6 mA current for 90 s.

support, leading to the formation of a thinner PA on the membrane surface during IP [11].

The results showed that all three support membranes can be categorized as hydrophilic (contact angle < 90°). The Upcycled PVC membrane showed a slightly more hydrophobic behavior than RG PVC membrane. This might be due to the existence of additives such as adipate and phthalate with a hydrophobic nature added to PVC pipe during its manufacturing [25]. The Upcycled PVC and RG PVC membranes showed slightly lower hydrophilicity than the PES membrane. The higher hydrophilicity of PES support is due to the highly electronegative oxygen atoms in PES, which make hydrogen bond with water molecules that are stronger than the dipole–dipole interactions between electronegative chlorine and water molecules in PVC membranes [33].

The surface charge of a support layer plays a crucial role in influencing the surface charge of the thin-film composite (TFC) membrane by exerting an impact on the polyamide (PA) structure. A support layer characterized by a more negative surface charge results in a corresponding increase in the negative surface charge of the TFC membrane [34,35]. The increased negative surface charge of the support layer can repel the negatively charged TMC, hindering its interaction with PIP. Consequently, this can lead to the formation of less crosslinking PA [34,35]. The surface charge of the three support membranes is presented in Fig. 2b. The Upcycled PVC membrane showed more negative surface charge than the other two membranes in a neutral pH range (5.5 – 8). The negative surface charge of Upcycled PVC and RG PVC membranes needs more investigation as due to their chemical structure, there is no possible dissociation or ionization that results in a negative surface charge. The more negative surface charge of the Upcycled PVC membrane compared to the RG PVC membrane may be attributed to the presence of additives, although it is not expected that common additives such as adipate, phthalate, and calcium carbonate in PVC pipe contribute to the enhanced surface charge since they are neutral by nature. However, the exact role of various PVC pipe additives in zeta potential remains unclear, and further investigation is required to understand their effect on zeta potential. Furthermore, surface roughness measurements of these membranes revealed that they exhibit similar surface average roughness (RG PVC (105 nm), Upcycled PVC (104 nm), and PES (107 nm) (Table S3). The MWCO and the average pore radius of membranes are shown in Fig. 3a and Table S2. The MWCO and the calculated pore size of all three membranes were in the range as reported for UF membranes in the literature [36,37]. All three membranes showed similar MWCO (top surface pore size). However, the Upcycled PVC and RG PVC membranes showed different pore morphology (Fig. 4 b and c). The SEM of RG PVC membrane showed a more porous sponge-like morphology compared to PES membrane with small pores throughout the cross-section. The SEM of the Upcycled PVC membrane showed a finger-like morphology with large pore size, lengths and volumes. In general, the pore size and pore morphology of a phase inverted membrane is a function of solvent/nonsolvent exchange rate [38]. The solvent-nonsolvent exchange rate in a phase inversion process is mainly influenced by the viscosity of the casting solution and the presence of additives. The viscosity of the dope solution impacts the exchange rate between solvent and nonsolvent during the demixing process and hence, influences the morphology of the resulting membrane. A higher viscosity of the dope solution hinders/slows down the exchange (diffusion) rate between solvent and nonsolvent, which results in delayed demixing leading to the formation of a dense and relatively thick top layer, less porous substructure and sponge-like morphology (less number of macrovoids in the porous sublayer) which further impact the membrane performance such as lower water flux [39,40]. On the contrary, lower viscosity of the casting solution accelerates the demixing of solvent and nonsolvent leading to the formation of a thin skin layer at the top and a

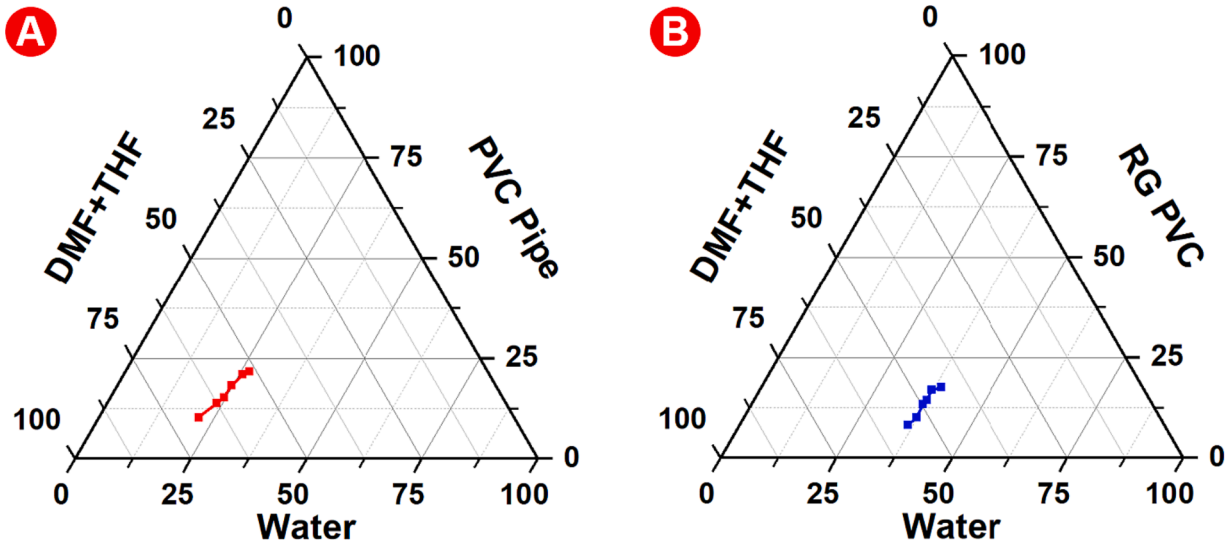

Fig. 5. Ternary phase diagrams for (a) PVC Pipe and (b) RG PVC at 23 °C in a solvent mixture of DMF: THF (3:2 V:V) and water as the non-solvent.

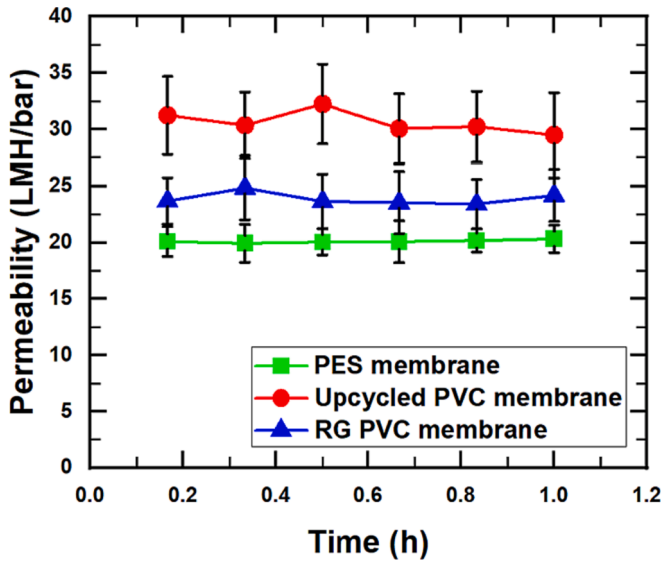

Fig. 6. Water permeability of PES, RG PVC, and Upcycled PVC support membranes. The membranes were compacted at 120 psi for 2 h. Water Permeability was measured at 100 psi for 1 h and permeate mass readings (g) were taken at 10-minute intervals.

finger-like morphology characterized by larger pore sizes, lengths, and volume [39,41]. The viscosity of the 22 wt% casting solutions of PVC pipe and RG PVC is presented in Fig. 3b. The results show that under identical casting solution preparation conditions, the viscosity of the RG PVC casting solution was higher than that of the PVC pipe casting solution. The reason for the lower viscosity of PVC pipe casting solution might be due to the presence of additives in PVC pipe, which were added to the PVC pipe during its manufacturing [27].

Generally, these additives disrupt the entanglements and interactions within the three-dimensional network of polymer chains, causing the PVC chains to loosen. This results in an increased amount of free space within the polymer matrix, allowing the chains to move more freely and thereby increasing their mobility. Consequently, this leads to a lower viscosity of the PVC material [42].

Since the PES membrane is a commercial membrane, there is no information about its fabrication condition.

The MWCO of all three membranes showed similar values in the range of 1500 to 1847.97 Da based on the more than 90 % rejection of PEG with 1500 MW. This trend suggests that all three membranes possessed a pore size (radius) of around 1.1 nm (Table S2). The rationale for this behavior could be attributed to the presence of hydrophobic additives, which may promote a reduction in pore size. This reduction compensates for the anticipated increase in pore size in the Upcycled PVC membrane with lower viscosity, as depicted in Fig. 3b.

The cloud point experiment was conducted to analyze the phase behavior of the ternary system of the polymer (PVC pipe and PVC RG) solvent and nonsolvent as a way to identify the effect of additives in PVC pipe regarding the solvent-nonsolvent interaction and consequently affecting the pore morphology (see supporting information S4). Fig. 5 shows the cloud point curves of PVC pipe and RG PVC within the DMF: THF/Water system. An observation from the graph is that the PVC pipe system (with the binodal curve positioned closer to the polymer–solvent axis) requires less amount of water (nonsolvent) to induce cloud point and phase separation compared to RG system (with the binodal curve situated nearer to the polymer-water axis). This distinction implies that the PVC pipe possessed lesser thermodynamic stability, which exhibited rapid demixing behavior (as explained based on the viscosity properties of the casting solution), resulting in a finger-like morphology (Fig. 4c). Conversely, RG PVC system possessed more thermodynamic stability imposing delayed demixing characteristics that consequently formed a sponge-like morphology (Fig. 4b) [43–45]. Since the only difference between the PVC pipe and RG PVC system was the presence of additives such as adipate and phthalate in PVC pipe, it can be inferred that these variations are attributed to the influence of additives in PVC pipe. It can be postulated that adipate and phthalate reduce polymer solubility by interacting with the solvent, thereby decreasing the amount of water required to precipitate the polymer [46,47].

3.2. Performance of the Upcycled PVC membrane (support layer)

The performance of the Upcycled PVC membranes was examined with reference to two control membranes, including RG PV membrane and commercial PES membrane. The water permeability results showed that the Upcycled PVC membrane had the highest pure water permeability, followed by the RG PVC membrane and then the PES membrane (Fig. 6). Generally, pore size, pore morphology and surface chemistry (i.e., surface hydrophilicity) determine the permeability of a membrane. Since all three membranes possessed almost a similar hydrophilicity and pore size (Figs. 2a and 3a), then the permeability behavior can be explained based on the morphology of these membranes. The distinctive finger-like morphology of the Upcycled PVC membranes is associated with reduced mass transfer resistance—essentially indicating a lesser hindrance to the flow of water molecules through the membrane. As a result of this favorable morphology, these membranes exhibited significantly higher permeability when compared to the other membranes. Likewise, the morphology of the RG PVC membrane exhibited lower mass transfer resistance in comparison to the sponge-like morphology of the PES membrane.

3.3. Characteristics of TFC membranes with Upcycled PVC support layer

Having covered the properties of the Upcycled PVC membrane in the preceding section, the subsequent discussion pertains to its utilization as the support layer for TFC membranes. The Polyamide layer (PA) forms atop the support layer through interfacial polymerization (IP). This occurs as piperazine molecules from the aqueous phase interact with TMC in the organic phase (n-hexane) at the interface. This interaction is initiated when the TMC organic phase is introduced onto the support, already bearing the absorbed aqueous phase containing piperazine monomers. Consequently, an amidation reaction ensues, giving rise to the polyamide layer [48]. The unreacted COCl groups from TMC undergo hydrolysis in water, resulting in the formation of carboxylic (–COOH) groups and generating HCl as a by-product [49,50].

The PA comprises both crosslinked and linear components. The crosslinking degree quantifies the proportion of crosslinked segments (amide bonds) relative to the linear segments (carboxylic groups) present in the polyamide layer on the support surface. A higher crosslinking degree signifies an increased presence of amide bonds and a reduced concentration of carboxylic groups within the polyamide layer [51,52]. This parameter holds significance due to its influence on PA layer void formation, membrane hydrophilicity, surface charge, pure water permeability, and salt rejection. A lower crosslinking degree corresponds to a higher number of voids inside the PA layer and an elevated carboxylic group content, which in turn leads to heightened hydrophilicity, more negative surface charge, increased permeability, and diminished salt rejection [53].

The crosslinking degree of PA depends on several factors, including the support layer physicochemical properties, the composition of the IP reaction mixture, the concentration of the reactants (such as the amine and acyl chloride), the reaction time and temperature, solvents type, and the presence of any additives or modifiers [11]. In this study, the same interfacial polymerization composition, duration, and temperature were consistently utilized across all membranes. Therefore, the influential factors contributing to variations in the characteristics of the PA layer were likely associated with the properties of the support layer, including aspects such as pore size/morphology, surface charge, and

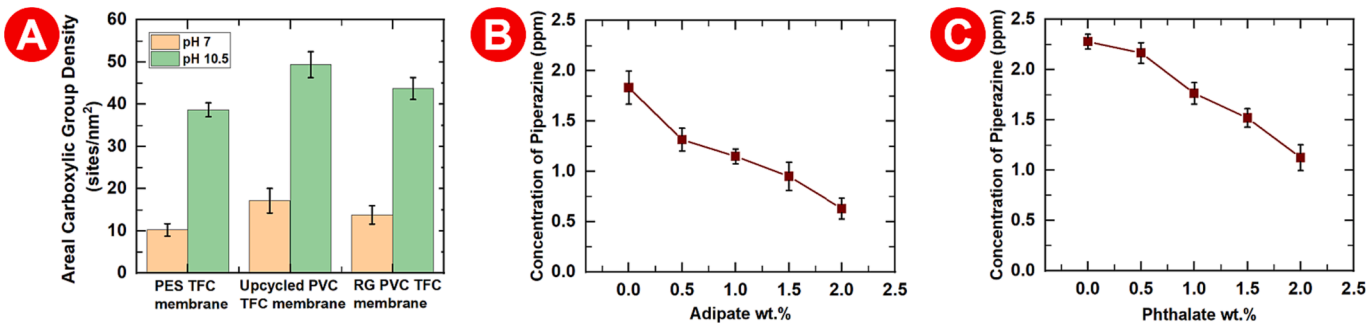

Fig. 7. (a) Areal carboxylic group density of TFC membranes with PES, Upcycled PVC and RG PVC support layer measured at pH = 7 and pH = 10.5 by performing silver binding and elution experiment, (b and c) PIP diffusion into the n-hexane solution within 30 s and in the presence of different concentrations of (b) adipate and (c) phthalate. The experiment was carried out at 23 °C with constant piperazine concentration (1 wt%) and varying adipate and phthalate concentration (0.5, 1,1.5 and 2 wt%) in the aqueous phase.

hydrophilicity. Varied pore sizes and morphologies among the support membranes result in distinct surface areas for polymerization. Consequently, the number of active sites available for interaction between piperazine (aqueous phase) and TMC (organic phase) differs, along with the penetration rates of the aqueous phase within the support layer. These factors contribute to the diversity in the crosslinking degrees. Support membranes featuring smaller pore sizes and a sponge-like morphology offer a larger surface area at the polymerization interface in comparison to their counterparts with larger pore sizes and a finger-like morphology. This expanded surface area facilitates the presence of a greater number of active sites, enabling piperazine (aqueous phase) to effectively interact with TMC (organic phase) and consequently leading to higher crosslinking degrees [54]. Furthermore, the combination of smaller pore sizes and a sponge-like morphology imposes challenges on the penetration of the piperazine aqueous phase within the support layer. As a result, the reaction between piperazine and TMC predominantly transpires at the support surface. This scenario translates to an increased concentration of piperazine molecules available on the surface, bolstering the interaction with TMC and fostering the formation of a more extensively crosslinked polyamide layer [48,55]. Conversely, larger pore sizes and the finger-like morphology characteristic of support membranes facilitate the penetration of the piperazine aqueous phase into the support layer. Consequently, a reduced number of piperazine molecules are accessible on the support surface to engage with TMC. This outcome culminates in the creation of a thinner and less crosslinked polyamide layer on the support surface [48]. With an elevated concentration of piperazine at the support surface, the impetus for piperazine to permeate through the initially established polyamide layer/film intensifies. This heightened driving force results in an augmented presence of piperazine molecules within the reaction zone—situated atop the initially formed polyamide film—primed to engage with TMC. Consequently, this dynamic drives polymerization, leading to the creation of an additional polyamide layer atop the initial thin polyamide film. This layered effect contributes to an overall increase in both the thickness and cross-linking degree of the polyamide layer [56,57].

The silver elution method was employed to measure the unreacted carboxylic groups of PA to determine PA degree of crosslinking [58,59]. The areal carboxylic group density of the three TFC membranes at pH = 7 and pH = 10.5 is shown in Fig. 7a. The carboxylic group density at pH = 7 represents the carboxyl (–COOH) groups on the PA surface, while the carboxylic group density at pH = 10.5 represents the carboxyl (–COOH) groups buried within the PA network [59]. Among the three TFC membranes, the PA layer formed on the top of the Upcycled PVC support layer had a higher carboxylic group density (lowest crosslinking degree) at both pHs, followed by RG PVC TFC and then PES TFC (highest crosslinking degree). The reason for this trend (as explained before) is attributed to the pore size and morphology of the support membranes.

In addition, another justification of the lower crosslinked degree of PA of the Upcycled PVC membranes might be due to the presence of adipate and phthalate (Fig. 1d). Adipate and phthalate compounds encompass ester groups (–COO), facilitating hydrogen bonding with the aqueous phase's (–NH) groups of piperazine and (–OH) groups of water molecules. This interaction introduces a counteracting force on the aqueous phase, thereby retarding its diffusion rate out of the support pores. Consequently, the availability of the aqueous phase reactant—piperazine molecules—diminishes, impeding their interaction with TMC (organic phase). This outcome yields a less crosslinked polyamide layer, indicative of a higher proportion of unreacted TMC (organic phase) [11,22,53,57]. To confirm this behavior, the interaction between pure adipate/phthalate and PIP was investigated experimentally (Fig. 7 b and c). As shown in Fig. 7 b and c, the concentration of

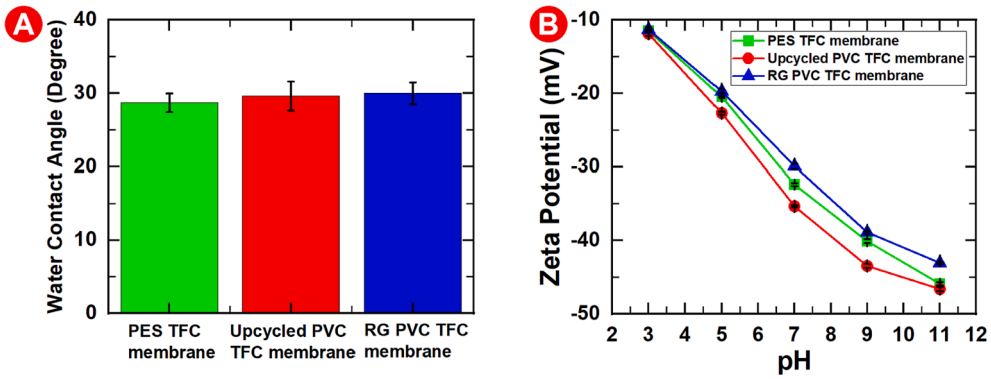

Fig. 8. (a) The water contact angle of TFC membranes with PES, Upcycled PVC and RG PVC support membranes measured at 20 different points on 3 different samples of the membranes and (b) Zeta Potential (Surface Charge) of TFC membranes with PES, Upcycled PVC and RG PVC support membranes.

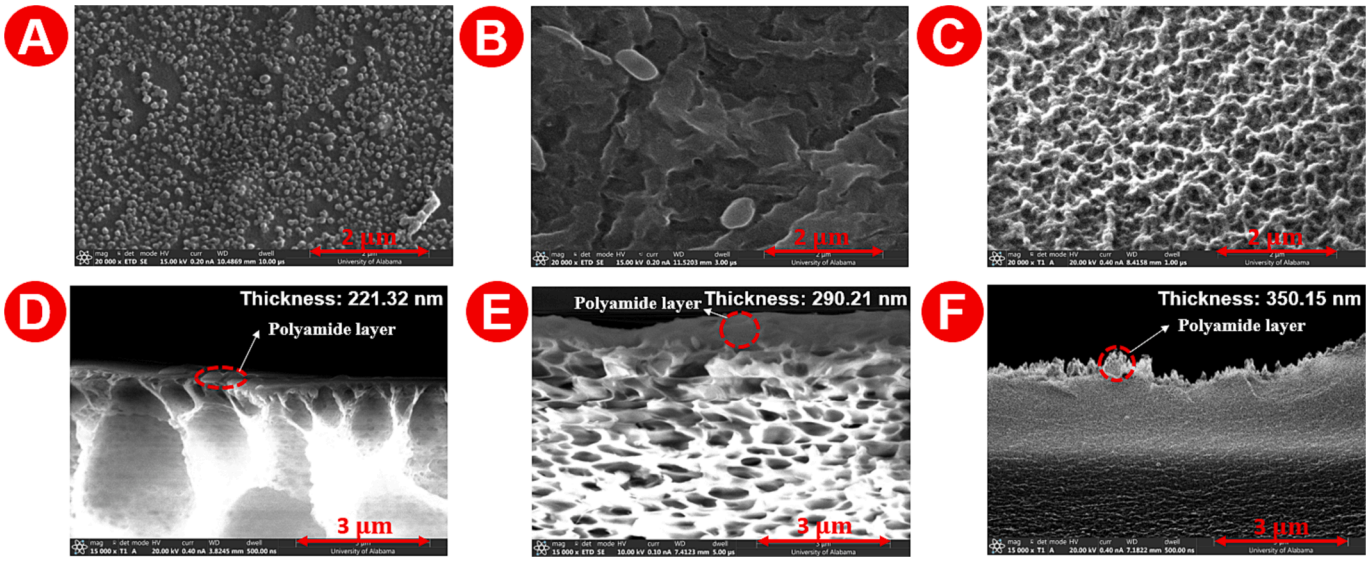

Fig. 9. The top surface and cross-sectional SEM images of (a and d) Upcycled PVC TFC, (b and e) RG PVC TFC and (c and f) PES TFC membranes fabricated on top of Upcycled PVC, RG PVC and PES support membranes, respectively.

piperazine diffusion into n-hexane (organic phase) decreased with an increase in the amount of adipate and phthalate. This confirms the interaction between adipate/phthalate and the aqueous phase, possibly via hydrogen bonding, which retarded (slowed down) the diffusion rate of piperazine out of the support pores.

The water contact angle of TFC membranes with the Upcycled PVC support layer was in range with TFC membranes fabricated using the commercial PES support layer (Fig. 8a). The TFC membranes showed hydrophilic properties due to the N–C=O groups (crosslinked section of PA layer) and –COOH groups (uncrosslinked section of PA), which make a hydrogen bonding with water molecules [60,61]. As all the TFC membranes possess a polyamide layer with N-C=O groups and nearly identical areal carboxylic group densities on the membrane surface at pH = 7 (Fig. 7a) their water contact angles are consequently similar. This result showed that the use of an Upcycled PVC membrane as the support layer of a TFC membrane did not affect the hydrophilicity of a PA layer compared to using a commercial PES support layer.

The three TFC membranes showed a similar surface charge (Fig. 8b), with a slightly more negative surface charge for TFC with an Upcycled PVC support layer at all pHs followed by RG PVC TFC and then PES TFC. The ZP trend can be explained based on the areal carboxylic group density (Fig. 7a) where the presence of more –COOH groups on the membrane surface resulted in a more negative surface charge of the membrane (Fig. 8b) [51,62]. The relatively more negative surface charge of the Upcycled PVC TFC membrane can be justified based on the higher amount of carboxylic groups on the surface of its PA layer, as confirmed by the silver elution analysis at pH 7 (Fig. 7a).

Fig. 9 shows the top surface and cross-section SEM images of Upcycled PVC, RG PVC, and PES TFC membranes. The TFC membrane with an Upcycled PVC support layer showed globular-like nodular morphology, RG PVC TFC membrane had a spread out (leaf-like) morphology, while PES TFC membrane had a ridge and valley structure. The reasons for these different morphologies of the TFC membranes can be related to the different physicochemical properties of the support layers [63,64]. In the case of Upcycled PVC, larger pore sizes and the finger-like morphology of the support membrane promoted the ingress of PIP into the support layer. As a result, there was a diminished number of PIP molecules available on the support surface for interaction with TMC [26]. The reduced PIP concentration on the support layer's surface fostered the creation of dispersed globules or nodules. These nodules were spaced apart, preventing their amalgamation, and resulting in the generation of smaller polyamide tufts.

Moreover, the lower PIP concentration on the support surface, combined with the slower diffusion rate of PIP into TMC, limits the growth of the tufts, ultimately leading to the formation of a thinner polyamide layer having an average thickness of 221.32 nm (as depicted in Fig. 9d) [65,66]. In addition, the morphology can likely be attributed to the presence of adipate and phthalates, which facilitated hydrogen bonding with PIP and water molecules. The consequence of this interaction was a diminished number of PIP molecules available to interact with TMC. This circumstance facilitated the formation of dispersed globules or nodules, with these nodules exhibiting spacing that prevented their fusion. Consequently, this led to the formation of smaller polyamide tufts (Fig. 9a). The TFC with RG PVC support layer with the absence of additives, smaller pore size and sponge-like morphology, showed closely packed globules/nodules that joined together, leading to the formation of spread out (leaf-like) polyamide layer on the support surface (Fig. 9b). The elevated concentration of PIP on the support surface, coupled with its rapid diffusion into TMC, culminated in a relatively thicker polyamide layer having an average thickness of 290.21 nm (Fig. 9e). For the PES TFC, the absence of additives, smaller pore size, and a more densely packed, sponge-like morphology in the

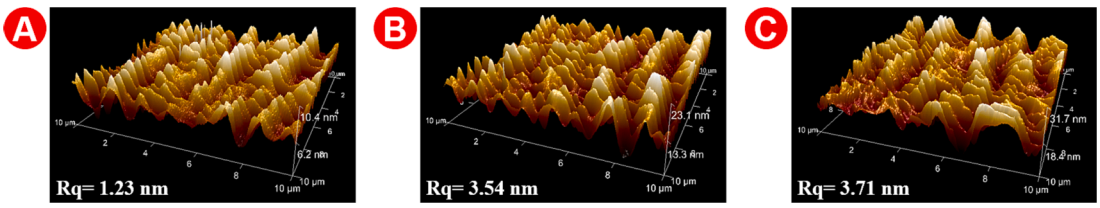

Fig. 10. AFM images of (a) PES TFC, (b) RG PVC TFC and (c) Upcycled PVC TFC. Surface roughness parameters of membranes obtained from analyzing three randomly chosen 20 µm × 20 µm AFM images.

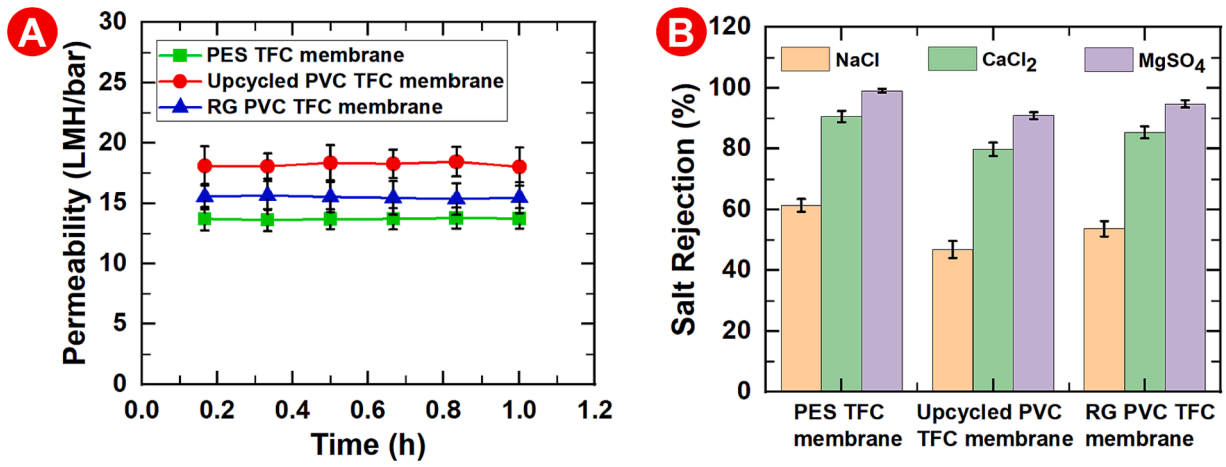

Fig. 11. (a) Water permeability of PES, Upcycled PVC, and RG PVC TFC membranes. Water permeability was measured at 100 psi for 1 h and permeate mass readings (g) were taken at 10-minute intervals, (b) Rejection of three salts (NaCl, $CaCl_2$ and $MgSO_4$) by PES, Upcycled PVC, and RG PVC TFC membranes. The initial concentration of the three salts was 2000 ppm.

PES support layer compared to the RG PVC support layer resulted in the highest concentration of piperazine on the support surface and the fastest diffusion rate of piperazine into TMC (organic phase). This fast diffusion led to the formation of densely packed globules/nodules that clustered together, forming a dense ridge and valley structure (Fig. 9c). Additionally, the significantly faster rate of piperazine diffusion into TMC for the PES support layer, compared to the RG PVC support layer, resulted in a much faster growth rate of the polyamide layer on the PES support. This, in turn, led to the formation of a thicker and more crosslinked polyamide layer on the PES support membrane, having an average thickness of 350.15 nm when compared to the RG PVC support membrane (Fig. 9f).

Fig. 10 depicts the surface roughness of the three TFC membranes. Notably, the TFC membranes with Upcycled and RG PVC support exhibited higher surface roughness compared to those with a PES support layer. This heightened roughness finds its explanation in the PA morphology, which was previously discussed. Specifically, the PA layer of PVC membranes displayed an increased presence of surface nodules, indicative of a greater number of discontinuities and irregularities when contrasted with the TFC PA on the PES support layer [67].

3.4. Performance of TFC membranes with Upcycled PVC support layer

The pure water permeability of the TFC membranes is illustrated in Fig. 11a. Among the membranes, those with Upcycled PVC support demonstrated the highest permeability, followed by RG PVC and TFC with the PES support layer. The permeability of TFC membranes is significantly influenced by two key factors: the thickness and crosslinking degree of the PA layer [11,68]. The heightened water permeability in TFC membranes with Upcycled PVC support can be attributed to their lower crosslinking degree (Fig. 7a), the dispersed spacing of globular/nodular-like surface morphology with smaller polyamide tufts (Fig. 9a), and a thinner polyamide layer (Fig. 9d), when compared to RG PVC and PES TFC membranes. Surface roughness also played a crucial role in determining the water permeability differences among the three TFC membranes. Upcycled PVC TFC and RG PVC TFC membranes exhibited the highest surface roughness, followed by RG PVC TFC and then PES TFC. The increased surface roughness in Upcycled PVC TFC membranes enlarged the effective membrane area and heightened the friction force between the membrane surface and water molecules. This, in turn, slowed down the flow of water molecules over the membrane surface and facilitated water molecule adhesion to the membrane. Consequently, the permeability of Upcycled PVC TFC membranes improved compared to RG PVC TFC and PES TFC membranes [69,70].

Fig. 11b illustrates the rejection of three salts—sodium chloride (NaCl), calcium chloride ($CaCl_2$), and magnesium sulfate ($MgSO_4$)—by the TFC membranes. Overall, all three membranes showed semi-similar and acceptable salt rejection as the NF membrane. The highest rejection rates for all three salts were observed in TFC membranes with a PES support layer, followed by TFC with RG PVC and Upcycled PVC support layers. Salt rejection in TFC membranes is influenced by size exclusion and surface charge mechanisms [43,71]. As all three membranes

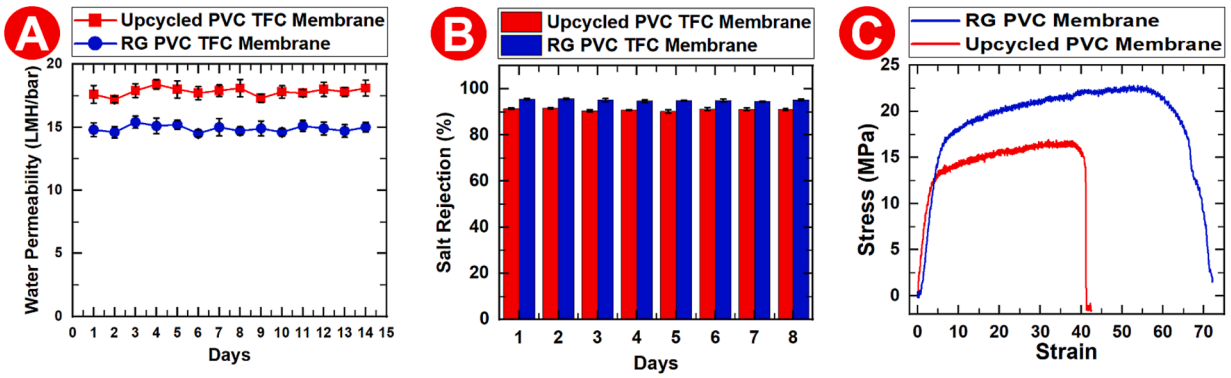

Fig. 12. (a) water permeability, (b) salt ($MgSO_4$) rejection, and (c) mechanical strength of Upcycled PVC (Red) and RG PVC (Blue) membranes. The water permeability tests were performed for 14 consecutive days, and the salt rejection experiments were performed for 8 consecutive days at a pressure of 100 psi. (For interpretation of the references to color in this figure legend, the reader is referred to the web version of this article.)

exhibited nearly equivalent surface charges (Fig. 8b), the determining factor in salt rejection was primarily the physical properties of the PA layer. The observed results can be rationalized by considering the PA thickness and crosslinking degree in the TFC membranes. TFC membranes with Upcycled PVC support possessed a thinner polyamide layer, as elaborated earlier in section 3.3 (Fig. 9d), along with a lower crosslinking degree (Fig. 7a) and higher permeability (Fig. 11a). These factors collectively led to reduced salt rejection in comparison to RG PVC and PES TFC membranes.

The results show that for all three TFC membranes, the rejection of $MgSO_4$ was the highest, followed by $CaCl_2$ and then NaCl. The salt rejection performance of the TFC membranes is controlled by two fundamental mechanisms, which are size exclusion and Donnan exclusion [51,72]. Among cations, Mg^{2+} has the highest hydrated ionic radius, followed by Ca^{2+} and then $Na^{+;}$ hence, based on size, the rejection follows the order of $Mg^{2+} > Ca^{2+} > Na^{+}$ [73–77]. Among anions, SO_4^{2-} has a higher hydrated ionic radius compared to Cl^- hence, the rejection follows the order of $SO_4^{2-} > Cl^-$ [74,76–79]. The surface of all three TFC membranes is negatively charged (Fig. 8b) and based on Donnan exclusion, sulfate ions SO_4^{2-} having a more negative charge than chloride ions (Cl^-) experience a much greater electrostatic repulsion and were rejected more compared to Cl^- ions; therefore $MgSO_4$ had a higher rejection than $CaCl_2$ and NaCl [51,80]. The performance of the Upcycled PVC TFC membrane was benchmarked and compared with other membranes reported in the literature (Table S4). The results indicate similar or superior performance of the Upcycled PVC TFC membranes.

3.5. Stability and pressure resistance of TFC membranes with Upcycled PVC support layer

The stability and pressure resistance of the Upcycled PVC TFC and RG PVC TFC membranes were studied by measuring their water permeability for 14 consecutive days and salt ($MgSO_4$) rejection for 8 consecutive days at a pressure of 100 psi. The results are shown in Fig. 12 a and b. The results show that the water permeability and salt rejection remain constant over the course of 14 and 8 days, respectively, demonstrating acceptable pressure resistance and stability. In addition, mechanical testing of the support membranes (Upcycled PVC and RG PVC) was performed to check their pressure resistance or maximum bearable stress. The results are presented in Fig. 12c. According to the results (Fig. 12c), both Upcycled PVC and RG PVC show excellent bearable stress levels of around 17 and 23 MPa, respectively.

4. Conclusions

In this study, we explored the upcycling of waste PVC pipe to create a support layer for Thin-Film Composite (TFC) membranes and compared the performance of these upcycled TFC membranes with conventional TFC membranes. The TFC membranes were synthesized through interfacial polymerization on three distinct support layers: upcycled waste PVC pipe, research-grade (RG) PVC, and commercially available polyethersulfone (PES) membranes and a comprehensive analysis of the physicochemical properties and performance of these three TFC membranes were conducted. It was found that while the three TFC membranes showed almost similar hydrophilicity and surface charge, their PA morphology, surface roughness, and performance in terms of pure water permeability and salt rejection differed which was attributed to the different support layer physicochemical properties (pore size, morphology, and the presence of additives) on which the TFC membranes were fabricated. Upcycled PVC support layer due to its larger pore size, finger-like morphology and the presence of additives resulted in the formation of thinner, less crosslinked, relatively defective, and smaller dispersed nodular-like polyamide structure with relatively higher surface roughness leading to higher pure water permeability and comparable/slightly lower salt rejection compared to RG PVC TFC and PES TFC. In summary, this study demonstrated that upcycling waste PVC pipe to create a support layer for TFC membranes yielded TFC membranes with comparable or even superior performance to TFC membranes fabricated on commercially available PES support layers. This innovative approach addresses two of the most pressing global challenges: plastic pollution and water purification/treatment, simultaneously.

CRediT authorship contribution statement

Atta Ur Razzaq: Conceptualization, Data curation, Formal analysis, Investigation, Methodology, Validation, Visualization, Writing – original draft, Writing – review & editing. **Milad Rabbani Esfahani:** Writing – review & editing, Visualization, Supervision, Resources, Methodology, Funding acquisition, Formal analysis, Data curation, Conceptualization.

Declaration of competing interest

The authors declare that they have no known competing financial interests or personal relationships that could have appeared to influence the work reported in this paper.

Data availability

Data will be made available on request.

Acknowledgements

The authors thank the National Science Foundation (NSF) for the financial support under Award No. 2029387. The authors thank Dr. S. Nima Mahmoodi for AFM imaging and Dr. Qiaoli Liang for LC-MS analysis. The authors gratefully thank the Department of Chemical and Biological Engineering at the University of Alabama, The Center for Water Quality Research (CWQR), and the Alabama Water Institute (AWI) at the University of Alabama for instrumental support.

Appendix A. Supplementary material

Supplementary data to this article can be found online at https://doi.org/10.1016/j.seppur.2024.126747.

References

[1] T.R. Walker, L. Fequet, Current trends of unsustainable plastic production and micro(nano)plastic pollution, TrAC Trends Anal. Chem. 160 (2023) 116984.
[2] G.G.N. Thushari, J.D.M. Senevirathna, Plastic pollution in the marine environment, Heliyon 6 (2020) e04709.
[3] A.A. Mamun, T.A.E. Prasetya, I.R. Dewi, M. Ahmad, Microplastics in human food chains: food becoming a threat to health safety, Sci. Total Environ. 858 (2023) 159834.
[4] P.W. Brandt-Rauf, Y. Li, C. Long, R. Monaco, G. Kovvali, M.J. Marion, Plastics and carcinogenesis: the example of vinyl chloride, J. Carcinog. 11 (2012) 5.
[5] A. Zulfi, S. Hartati, S. Nur'aini, A. Noviyanto, M. Nasir, Electrospun nanofibers from waste polyvinyl chloride loaded silver and titanium dioxide for water treatment applications, ACS Omega 8 (2023) 23622–23632.
[6] K. Lewandowski, K. Skórczewska, A brief review of Poly(Vinyl Chloride) (PVC) recycling, Polymers 14 (2022) 3035.
[7] X. Chen, X. Bai, Co-conversion of wood and polyvinyl chloride to valuable chemicals and high-quality solid fuel, Waste Manag. 144 (2022) 376–386.
[8] Q. Hou, M. Zhen, H. Qian, Y. Nie, X. Bai, T. Xia, M. Laiq Ur Rehman, Q. Li, M. Ju, Upcycling and catalytic degradation of plastic wastes, Cell Rep. Phys. Sci. 2 (2021) 100514.
[9] Z. Alihemati, T. Matsuura, A. Ismail, N. Hilal, Current status and challenges of fabricating thin film composite forward osmosis membrane: a comprehensive roadmap, Desalination 491 (2020).
[10] N. Misdan, W.J. Lau, A. Ismail, Physicochemical characteristics of poly(piperazine-amide) TFC nanofiltration membrane prepared at various reaction times and its relation to the performance, J. Polym. Eng. 35 (2014) 71.
[11] H. Mokarizadeh, S. Moayedfard, M.S. Maleh, S.I.G.P. Mohamed, S. Nejati, M. R. Esfahani, The role of support layer properties on the fabrication and

performance of thin-film composite membranes: the significance of selective layer-support layer connectivity, Sep. Purif. Technol. 278 (2021) 119451.
[12] S.H. Park, Y.J. Kim, S.J. Kwon, M.G. Shin, S.E. Nam, Y.H. Cho, Y.I. Park, J.F. Kim, J.-H. Lee, Polyethylene battery separator as a porous support for thin film composite organic solvent nanofiltration membranes, ACS Appl. Mater. Interfaces 10 (2018) 44050–44058.
[13] H.I. Kim, S.S. Kim, Plasma treatment of polypropylene and polysulfone supports for thin film composite reverse osmosis membrane, J. Membr. Sci. 286 (2006) 193–201.
[14] S. Li, C. Li, X. Song, B. Su, B. Mandal, B. Prasad, X. Gao, C. Gao, Graphene quantum dots-doped thin film nanocomposite polyimide membranes with enhanced solvent resistance for solvent-resistant nanofiltration, ACS Appl. Mater. Interfaces 11 (2019) 6527–6540.
[15] E.-S. Kim, Y.J. Kim, Q. Yu, B. Deng, Preparation and characterization of polyamide thin-film composite (TFC) membranes on plasma-modified polyvinylidene fluoride (PVDF), J. Membr. Sci. 344 (2009) 71–81.
[16] Z. Zhai, C. Jiang, N. Zhao, W. Dong, P. Li, H. Sun, Q.J. Niu, Polyarylate membrane constructed from porous organic cage for high-performance organic solvent nanofiltration, J. Membr. Sci. 595 (2020) 117505.
[17] C. Ji, Z. Zhai, C. Jiang, P. Hu, S. Zhao, S. Xue, Z. Yang, T. He, Q.J. Niu, Recent advances in high-performance TFC membranes: a review of the functional interlayers, Desalination 500 (2021) 114869.
[18] W.-J. Lau, G.-S. Lai, J. Li, S. Gray, Y. Hu, N. Misdan, P.-S. Goh, T. Matsuura, I. W. Azelee, A.F. Ismail, Development of microporous substrates of polyamide thin film composite membranes for pressure-driven and osmotically-driven membrane processes: a review, J. Ind. Eng. Chem. 77 (2019) 25–59.
[19] M. He, T. Yuan, W. Dong, P. Li, Q. Jason Niu, J. Meng, High-performance acid-stable polysulfonamide thin-film composite membrane prepared via spinning-assist multilayer interfacial polymerization, J. Mater. Sci. 54 (2019) 886–900.
[20] D. Menne, C. Üzüm, A. Koppelmann, J. Wong, C. Foeken, F. Borre, L. Dähne, T. Laakso, A. Pihlajamäki, M. Wessling, Regenerable polymer/ceramic hybrid nanofiltration membrane based on polyelectrolyte assembly by layer-by-layer technique, J. Membr. Sci. 520 (2016).
[21] S. De, M. Mondal, Characterization and antifouling properties of polyethylene glycol added PAN-CAP blend membrane, RSC Adv. 5 (2015).
[22] N. Misdan, W.J. Lau, A.F. Ismail, T. Matsuura, D. Rana, Study on the thin film composite poly(piperazine-amide) nanofiltration membrane: Impacts of physicochemical properties of substrate on interfacial polymerization formation, Desalination 344 (2014) 198–205.
[23] A. Ul-Hamid, K. Al-Soufi, L. Al-Hadhrami, A. Shemsi, Failure investigation of an underground low voltage XLPE insulated cable, Anti-Corros. Methods Mater. 62 (2015) 281–287.
[24] M. Pandey, G. Joshi, A. Mukherjee, P. Thomas, Electrical properties and thermal degradation of poly(vinyl chloride)/polyvinylidene fluoride/ZnO polymer nanocomposites, Polym. Int. (2016).
[25] I.N. Vikhareva, G.K. Aminova, A.K. Mazitova, Ecotoxicity of the adipate plasticizers: influence of the structure of the alcohol substituent, Molecules 26 (2021).
[26] A. Marcilla, S. García, J.C. García-Quesada, Study of the migration of PVC plasticizers, J. Anal. Appl. Pyrol. 71 (2004) 457–463.
[27] A. Ur Razzaq, D.J. McEachern, P.A. Rupar, P.R. Willis, S.N. Mahmoodi, M. R. Esfahani, Upcycled Polyvinyl Chloride (PVC) electrospun nanofibers from waste PVC-based materials for water treatment, ACS Appl. Eng. Mater. (2023).
[28] G.-B. Cai, S. Chen, L. Liu, J. Jiang, H.-B. Yao, A.-W. Xu, S.-H. Yu, 1,3-Diamino-2-hydroxypropane-N, N, N′, N′-tetraacetic acid stabilized amorphous calcium carbonate: nucleation, transformation and crystal growth, CrstEngComm 12 (2010).
[29] S. Mouanni, D. Amitouche, T. Mazari, C.H. Rabia, Transition metal-substituted Keggin-type polyoxometalates as catalysts for adipic acid production, Appl. Petrochem. Res. 9 (2019).
[30] M. Gao, X. Gong, M. Lv, W. Song, X. Ma, Y. Qi, L. Wang, Effect of temperature and pH on the sorption of dibutyl phthalate on humic acid, Water Air Soil Pollut. 227 (2016).
[31] N.A. Alenazi, M.A. Hussein, K.A. Alamry, A.M. Asiri, Nanocomposite-based aminated polyethersulfone and carboxylate activated carbon for environmental application, A Real Sample Anal. C 4 (2018) 30.
[32] H. Karimi, A. Rahimpour, M.R. Shirzad Kebria, Pesticides removal from water using modified piperazine-based nanofiltration (NF) membranes, Desalin. Water Treat. 57 (2016) 1–11.
[33] P. Kallem, G. Bharath, K. Rambabu, C. Srinivasakannan, F. Banat, Improved permeability and antifouling performance of polyethersulfone ultrafiltration membranes tailored by hydroxyapatite/boron nitride nanocomposites, Chemosphere 268 (2021) 129306.
[34] C. Liu, W. Wang, L. Zhu, F. Cui, C. Xie, X. Chen, N. Li, High-performance nanofiltration membrane with structurally controlled PES substrate containing electrically aligned CNTs, J. Membr. Sci. 605 (2020) 118104.
[35] H.-R. Chae, C.-H. Lee, P.-K. Park, I.-C. Kim, J.-H. Kim, Synergetic effect of graphene oxide nanosheets embedded in the active and support layers on the performance of thin-film composite membranes, J. Membr. Sci. 525 (2017) 99–106.
[36] A. Schaefer, R. Mauch, T. Waite, A.G. Fane, Charge effects in the fractionation of natural organics using ultrafiltration, Environ. Sci. Tech. 36 (2002) 2572–2580.
[37] A. Cassano, C. Conidi, R. Ruby-Figueroa, R. Castro-Muñoz, Nanofiltration and tight ultrafiltration membranes for the recovery of polyphenols from agro-food by-products, Int. J. Mol. Sci. 19 (2018).
[38] A.K. Hołda, I.F.J. Vankelecom, Understanding and guiding the phase inversion process for synthesis of solvent resistant nanofiltration membranes, J. Appl. Polym. Sci. 132 (2015).
[39] N. Ismail, N. Jakariah, N. Bolong, S. Anissuzaman, N.A.H.M. Nordin, A. Razali, Effect of polymer concentration on the morphology and mechanical properties of asymmetric polysulfone (PSf) membrane, J. Appl. Membr. Sci. Technol. 21 (2017).
[40] S. Hamzah, N. Aini, M. Ariffin, A. Ali, A. Mohammad, High performance of polysulfone ultrafiltration membrane: effect of polymer concentration, J. Eng. Appl. Sci. 9 (2014).
[41] B. Zhou, Simulations of polymeric membrane formation in 2D and 3D, in: Department of Materials Science and Engineering at the Massachusetts Institute of Technology, Massachusetts Institute of Technology, 2006, pp. 1–213.
[42] J. Czogała, E. Pankalla, R. Turczyn, Recent attempts in the design of efficient PVC plasticizers with reduced migration, Materials (Basel) 14 (2021).
[43] Z. Maghsoud, M.H.N. Famili, S.S. Madaeni, Preparation of polyvinylchloride membranes from solvent mixture by immersion precipitation, J. Appl. Polym. Sci. 131 (2014).
[44] M. Sadrzadeh, S. Bhattacharjee, Rational design of phase inversion membranes by tailoring thermodynamics and kinetics of casting solution using polymer additives, J. Membr. Sci. 441 (2013) 31–44.
[45] S. Mazinani, S. Darvishmanesh, A. Ehsanzadeh, B. Van der Bruggen, Phase separation analysis of Extem/solvent/non-solvent systems and relation with membrane morphology, J. Membr. Sci. 526 (2017) 301–314.
[46] M.A. Aroon, A.F. Ismail, M.M. Montazer-Rahmati, T. Matsuura, Morphology and permeation properties of polysulfone membranes for gas separation: effects of non-solvent additives and co-solvent, Sep. Purif. Technol. 72 (2010) 194–202.
[47] M. Yousefian-Arani, A. Sharif, M. Karimi, Thermodynamic analysis of polymeric membrane formation by non-solvent induced phase separation in the presence of different nanoparticles, J. Mol. Liq. 362 (2022) 119732.
[48] F. Liu, L. Wang, D. Li, Q. Liu, B. Deng, A review: the effect of the microporous support during interfacial polymerization on the morphology and performances of a thin film composite membrane for liquid purification, RSC Adv. 9 (2019) 35417–35428.
[49] W.J. Lau, Polyamide (PA), in: E. Drioli, L. Giorno (Eds.), Encyclopedia of Membranes, Springer, Berlin Heidelberg, Berlin, Heidelberg, 2015, pp. 1–3.
[50] H. Liu, M. Zhang, H. Zhao, Y. Jiang, G. Liu, J. Gao, Enhanced dispersibility of metal-organic frameworks (MOFs) in the organic phase via surface modification for TFN nanofiltration membrane preparation, RSC Adv. 10 (2020) 4045–4057.
[51] L.F. Liu, X. Huang, X. Zhang, K. Li, Y.L. Ji, C.Y. Yu, C.J. Gao, Modification of polyamide TFC nanofiltration membrane for improving separation and antifouling properties, RSC Adv. 8 (2018) 15102–15110.
[52] A. Tayefeh, R. Poursalehi, M. Wiesner, S.A. Mousavi, XPS study of size effects of Fe3O4 nanoparticles on crosslinking degree of magnetic TFN membrane, Polym. Test. 73 (2019) 232–241.
[53] R. Xu, G. Xu, J. Wang, J. Chen, F. Yang, J. Kang, M. Xiang, Influence of l-lysine on the permeation and antifouling performance of polyamide thin film composite reverse osmosis membranes, RSC Adv. 8 (2018) 25236–25247.
[54] L. Huang, J.R. McCutcheon, Impact of support layer pore size on performance of thin film composite membranes for forward osmosis, J. Membr. Sci. 483 (2015) 25–33.
[55] J.J. Beh, E.P. Ng, J.Y. Sum, B.S. Ooi, Thermodynamics and kinetics control of support layer synthesis for enhanced thin film composite membrane performance, J. Appl. Polym. Sci. 135 (2018) 45802.
[56] B. Khorshidi, T. Thundat, B.A. Fleck, M. Sadrzadeh, Thin film composite polyamide membranes: parametric study on the influence of synthesis conditions, RSC Adv. 5 (2015) 54985–54997.
[57] S.-J. Park, S.J. Kwon, H.-E. Kwon, M.G. Shin, S.-H. Park, H. Park, Y.-I. Park, S.-E. Nam, J.-H. Lee, Aromatic solvent-assisted interfacial polymerization to prepare high performance thin film composite reverse osmosis membranes based on hydrophilic supports, Polymer 144 (2018) 159–167.
[58] D. Chen, J.R. Werber, X. Zhao, M. Elimelech, A facile method to quantify the carboxyl group areal density in the active layer of polyamide thin-film composite membranes, J. Membr. Sci. 534 (2017) 100–108.
[59] C. Boo, Y. Wang, I. Zucker, Y. Choo, C.O. Osuji, M. Elimelech, High performance nanofiltration membrane for effective removal of perfluoroalkyl substances at high water recovery, Environ. Sci. Tech. 52 (2018) 7279–7288.
[60] N.S. Murthy, Hydrogen bonding, mobility, and structural transitions in aliphatic polyamides, J. Polym. Sci. B 44 (2006) 1763–1782.
[61] H. Shinzawa, J. Mizukado, Water absorption by polyamide (PA) 6 studied with two-trace two-dimensional (2T2D) near-infrared (NIR) correlation spectroscopy, J. Mol. Struct. 1217 (2020) 128389.
[62] P.S. Singh, A.P. Rao, P. Ray, A. Bhattacharya, K. Singh, N.K. Saha, A.V.R. Reddy, Techniques for characterization of polyamide thin film composite membranes, Desalination 282 (2011) 78–86.
[63] A.K. Ghosh, E.M.V. Hoek, Impacts of support membrane structure and chemistry on polyamide–polysulfone interfacial composite membranes, J. Membr. Sci. 336 (2009) 140–148.
[64] P. Veerababu, B.B. Vyas, P.S. Singh, P. Ray, Limiting thickness of polyamide–polysulfone thin-film-composite nanofiltration membrane, Desalination 346 (2014) 19–29.
[65] M.F. Jimenez Solomon, Y. Bhole, A.G. Livingston, High flux membranes for organic solvent nanofiltration (OSN)—Interfacial polymerization with solvent activation, J. Membr. Sci. 423–424 (2012) 371–382.
[66] Q. Dai, Z. Liu, L. Huang, C. Wang, Y. Zhao, Q. Fu, A. Zheng, H. Zhang, X. Li, Thin-film composite membrane breaking the trade-off between conductivity and selectivity for a flow battery, Nat. Commun. 11 (2020) 13.

[67] K. Tang, L. Zhu, P. Lan, Y. Chen, Z. Chen, Y. Lan, W. Lan, Regulating the thickness of nanofiltration membranes for efficient water purification, Nanoscale Adv. 5 (2023) 4770–4781.
[68] B. Khorshidi, T. Thundat, B.A. Fleck, M. Sadrzadeh, A novel approach toward fabrication of high performance thin film composite polyamide membranes, Sci. Rep. 6 (2016) 22069.
[69] M. Hirose, H. Ito, Y. Kamiyama, Effect of skin layer surface structures on the flux behaviour of RO membranes, J. Membr. Sci. 121 (1996) 209–215.
[70] Z. Zhong, D. Li, B. Zhang, W. Xing, Membrane surface roughness characterization and its influence on ultrafine particle adhesion, Sep. Purif. Technol. 90 (2012) 140–146.
[71] X. Zhang, J. Tian, Z. Ren, W. Shi, Z. Zhang, Y. Xu, S. Gao, F. Cui, High performance thin-film composite (TFC) forward osmosis (FO) membrane fabricated on novel hydrophilic disulfonated poly(arylene ether sulfone) multiblock copolymer/ polysulfone substrate, J. Membr. Sci. 520 (2016) 529–539.
[72] N.S. Suhalim, N. Kasim, E. Mahmoudi, I.J. Shamsudin, A.W. Mohammad, F. Mohamed Zuki, N.L. Jamari, Rejection mechanism of ionic solute removal by nanofiltration membranes: an overview, Nanomaterials (Basel) 12 (2022).
[73] J. Luo, S. Ye, T. Li, E. Sarnello, H. Li, T. Liu, Distinctive trend of metal binding affinity via hydration shell breakage in nanoconfined cavity, J. Phys. Chem. C 123 (2019) 14825–14833.
[74] C. Zhong, D. Yida, W. Hu, J. Qiao, L. Zhang, J. Zhang, A review of electrolyte materials and compositions for electrochemical supercapacitors, Chem. Soc. Rev. 44 (2015) 7431–7920.
[75] X. Zheng, J. Dou, J. Yuan, W. Qin, X. Hong, A. Ding, Removal of Cs+ from water and soil by ammonium-pillared montmorillonite/Fe3O4 composite, J. Environ. Sci. 56 (2017) 12–24.
[76] F. Liu, L. Wang, D. Li, Q. Liu, B. Deng, Preparation and characterization of novel thin film composite nanofiltration membrane with PVDF tree-like nanofiber membrane as composite scaffold, Mater. Des. 196 (2020) 109101.
[77] W. Shao, C. Liu, T. Yu, Y. Xiong, Z. Hong, Q. Xie, Constructing positively charged thin-film nanocomposite nanofiltration membranes with enhanced performance, Polymers (Basel) 12 (2020).
[78] I. Louati, F. Guesmi, A. Chaabouni, C. Hannachi, B. Hamrouni, Effect of ionic strength on the ion exchange equilibrium between AMX membrane and electrolyte solutions, Water Qual. Res. J. Can. 51 (2016).
[79] C. Kikuchi, H. Kurane, T. Watanabe, M. Demura, T. Kikukawa, T. Tsukamoto, Preference of Proteomonas Sulcata Anion Channelrhodopsin for Nitrate Revealed Using a pH Electrode Method, 2021.
[80] Y.W. Siew, K.L. Zedda, S. Velizarov, Nanofiltration of simulated acid mine drainage: effect of ph and membrane charge, Appl. Sci. 10 (2020) 400.

Supporting Information

Upcycled PVC support layer from waste PVC pipe for thin film composite nanofiltration membranes

Atta Ur Razzaq [a], Milad Rabbani Esfahani [a*]

[a] Department of Chemical and Biological Engineering, University of Alabama, Tuscaloosa 35487, United States

*Corresponding Author:
Milad Rabbani Esfahani
mesfahani@eng.ua.edu
Phone# 205-348-8836

Table of Contents

S1. Number-Average Molecular Weight (M_n) (g/mol), Weight Average Molecular Weight (M_w) (g/mol), and PDI of the PVC Pipe and RG PVC measured Using GPC.

Table S1. Number-Average Molecular Weight (M_n) (g/mol), Weight Average Molecular Weight (M_w) (g/mol), and PDI of the PVC Pipe and RG PVC measured Using GPC

Polymer	M_n	M_w	PDI
PVC Pipe	67,019	147,570	2.2
RG PVC	90,664	175,451	1.9

S2. Permeability and Salt Rejections of the Support and TFC Membranes.

The permeability was measured for 1 h by recording the mass of permeate collected after every 10 minutes. The permeability was calculated using the following formulas [1-3]:

$$J = \frac{Q}{A \times \Delta t} \qquad (1)$$

$$Per = \frac{J}{\Delta P} \qquad (2)$$

Where J is the pure water flux (L/m^2h), Q is the volume of permeate collected (L), Δt is the permeation or sampling time (h), A is the effective membrane area (m^2), Per is the pure water permeability ($L/m^2.h.bar$) and ΔP is the transmembrane pressure (bar).

The salt rejection of the TFC membranes was measured by passing 2000 ppm aqueous solutions of three salts sodium chloride (NaCl), calcium chloride ($CaCl_2$) and magnesium sulfate ($MgSO_4$) through the membrane in the cross-flow cell at 100 psi one at a time followed by washing the cell and membrane with DI water before passing the next salt through the membrane. The permeate for each salt was collected and the conductivity of feed (C_F) and permeate (C_P) salt solutions was measured. The salt rejection was calculated using [4]:

$$\% \, Rejection = \frac{C_F - C_P}{C_F} \times 100 \qquad (3)$$

S3. Molecular Weight Cutoff (MWCO) Measurements of the Support Membranes.

The smallest molecular weight of a solute (here polyethylene glycol (PEG)) that the membrane can retain by 90 % is known as the molecular weight cutoff (MWCO) of the membrane [5]. The molecular weight cutoff (MWCO) of the support membranes was measured using polyethylene glycol (PEG) with molecular weights 400, 600, 1000, 1500 and 2000 Da. For each molecular weight 1000 ppm solution of aqueous PEG was prepared. The support membrane was placed in a dead-end cell and the solutions were filtered (passed) through the membrane one molecular weight at a time in ascending order from lowest molecular weight (400 Da) to highest molecular weight (2000 Da) at a pressure of 60 psi. The filtration system was thoroughly cleaned with DI water between filtrations of different molecular weight PEG solutions. For each PEG molecular weight solution, the filtration test was run for 30 minutes before collecting the permeate to make sure that the system had reached steady state. The concentrations of feed and permeate solutions were determined using total organic carbon (TOC) analyzer [6]. The PEG retention percentage was calculated using [7]:

$$\% \, \text{Retention} = 1 - \frac{C_P}{C_0} \qquad (4)$$

Where C_P and C_0 are the concentrations of PEG in the permeate and feed, respectively. The molecular weight cutoff (MWCO) of the membrane, indicating the smallest molecular weight of a solute (in this case, polyethylene glycol or PEG) retained by the membrane at 90% efficiency, was determined by plotting % retention against PEG molecular weights [5]. Subsequently, the average pore radius of the membrane was calculated using the following formula based on the MWCO of the membranes [8]:

$$r_H = 0.06127(MW)^{0.3931} \quad (5)$$

Table S2. Molecular weight cutoff (MWCO) and average pore radius of PES, Upcycled PVC, and RG PVC support membranes.

Support Membrane	MWCO (Da)	Average Pore Radius (nm)
PES	1500	1.09
Upcycled PVC	1847.97	1.18
RG PVC	1671.04	1.13

S4. Determination of the Cloud Point Curve.

The ternary phase diagrams for PVC pipe and RG PVC casting solutions were constructed using the cloud point data obtained experimentally by the titration method. For both PVC pipe and RG PVC, six casting solutions with different concentrations (18,19,20,21,22 and 23 wt.%) were prepared by dissolving the appropriate amount of PVC pipe and RG PVC in DMF and THF in volume ratios of 3:2 and stirring the solutions at 400 rpm at 23 °C for 19 h followed by degassing for 4 h. Titration was performed by adding distilled water drop wise to each casting solution while stirring. When the first sign of turbidity appeared, the addition of distilled water was stopped, and the cloudy solution was stirred for an additional 30 min to see whether the turbid solution became clear. If the suspension remained turbid, the composition was recorded as the cloud point, but if the solution became clear, more water was added, and the process repeated. The composition at the cloud point was determined from the mass of the polymer, solvent (DMF:THF) and nonsolvent (water) present in the solution [9, 10].

S5. Silver Binding and Elution Method to Determine the Areal Carboxyl Group Density of the TFC Membranes.

Silver elution method was used to measure the carboxylic group density of the polyamide layer. This method consists of three steps: binding the silver ions to the ionized carboxyl groups, rinsing, or removing excess unbound silver ions from the membrane surface and protonating the carboxyl groups and eluting the bound silver ions. 10 mM silver nitrate stock solution was prepared by dissolving it in 1 wt.% nitric acid solution. This stock solution was diluted to 40 and 1 μM using DI water. The 40 μM solution was used for silver binding and 1 μM solution was used for rinsing i.e., removing excess un-attached silver ions on the membrane surface. The pH of the solutions was adjusted to 7 and 10.5 using 1 wt.% nitric acid solution and 0.1 M sodium hydroxide solution. The stored TFC membranes were taken out of the DI water and a square piece with an area of 2.25 cm^2 (L: 1.5 cm x W: 1.5 cm) was cut from each membrane. Each TFC membrane was then immersed in 10 mL of 40 μM silver nitrate solution for 10 minutes at pH 7 and 10.5. The membrane was then taken out and immersed in a second 10 mL of 40 μM silver nitrate solution for 10 minutes to bind silver ions one-to-one with the ionized carboxyl groups. Then the membrane was taken out and immersed 4 times, each time for 7 minutes, in 10 mL of 1 μM silver nitrate solution at the same pH used during the silver binding experiment to remove or rinse off excess un-attached silver ions on the membrane surface. After each step, the TFC membranes were lightly touched against kimwipes to reduce solution carryover. Finally, the TFC membranes were immersed in 5 mL of 1 wt.% solution of nitric acid for 30 minutes to protonate the carboxyl groups and elute the bound silver ions. The membrane was then taken out of the nitric acid solution and the concentration of the eluted silver ions in the solution was measured using ICP-OES [11, 12]. To convert the silver ion concentration measured using ICP to areal carboxyl group density, it was assumed that silver

ions have one-to-one binding with the ionized carboxyl groups i.e., one silver ion binds to one ionized carboxyl group; therefore, each eluted ion corresponds to one ionized carboxyl group. Also, it was assumed that within the polyamide film, all carboxyl groups could be accessed by silver ions. The concentration of ionized carboxyl groups is given by [12]:

$$[R - COO^-] = \frac{C_{Ag^+} V_{Ag^+} N_A}{A} \qquad (6)$$

Where, $[R - COO^-]$ is the areal density of the ionized carboxylic groups i.e. number of ionized carboxyl groups per unit area, A is the projected surface area of the polyamide film (surface area of one side of the membrane sample, neglecting surface roughness), C_{Ag^+} is the concentration of the eluted silver ions measured using ICP-OES, V_{Ag^+} is the elution volume, and N_A is the avagadro's constant/number (6.022 x 10^{23} mol^{-1}) [12].

S6. Average Thickness of the Upcycled PVC, RG PVC and PES Support Layers.

The thickness of the supporting layer plays a crucial role in influencing the development of the PA layer during the process of transporting PIP towards the TMC at the interface. Generally, a greater thickness in the support layer creates a more extensive cavity for the aqueous phase to infiltrate within the membrane pores. Consequently, this leads to an elongated pathway and increased duration for the aqueous phase to diffuse towards the reaction zone during the IP process. As a result of this delayed transport and extended pathway, the PA formed on the membrane surface tends to be thinner and exhibits fewer crosslinks. In this regard, the thickness of the phase-inverted membranes and the commercial PES membrane (control sample) was measured to evaluate their impact on the IP process. The measurement of thickness was conducted at ten distinct points on a single membrane sheet, and a minimum of three separate membrane sheets were subjected to examination (**Figure S1)**.

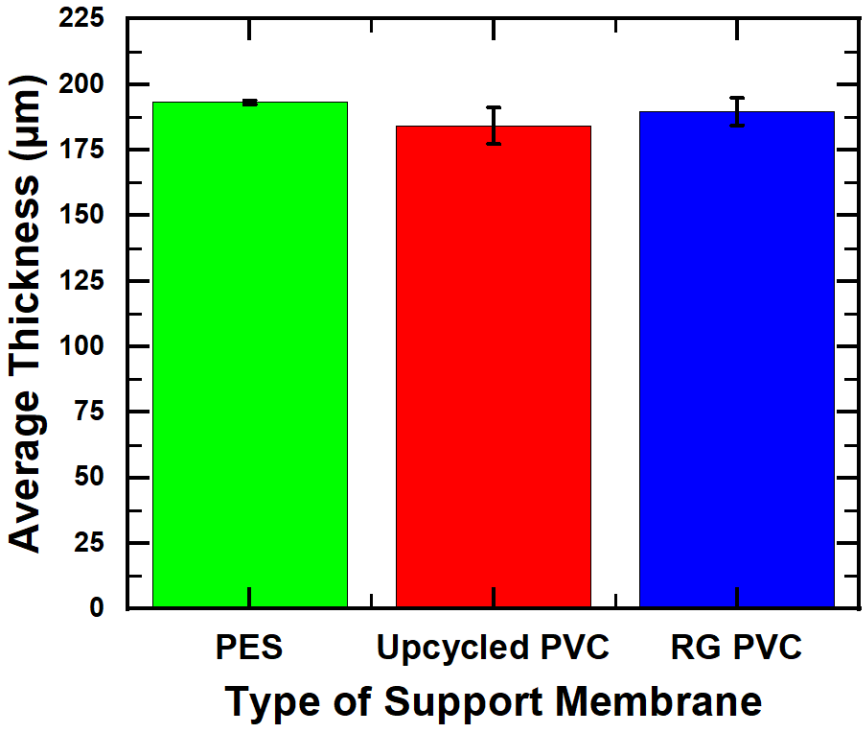

Figure S1. The average thickness of PES, Upcycled PVC and RG PVC membranes was measured at ten different points of a minimum of three membrane sheets. The measurement was conducted on membranes after immersion in water for 24 h.

The thickness of the commercial PES support membrane with the nonwomen was around 193 ± 0.79 µm, and the Upcycled PVC and RG PVC membranes showed a thickness of 184 ± 6.98 and 190 ± 5.23 µm respectively, which were in the same range and, therefore their thickness should not have had any effect on the formation of PA layer.

S7. Surface roughness of the support membranes.

Table S3. Surface roughness of Upcycled PVC, RG PVC and PES support membranes.

Type of Support Membrane	Average roughness (R_a) (nm)	Root Mean Square (RMS) roughness (R_q) (nm)
Upcycled PVC	104	134
RG PVC	105	135
PES	107	124

S8. Comparison of the commercial state-of-the-art TFC membranes to the TFC membranes used in this study.

Table S4. Comparative analysis of the TFC membranes employed in this study with commercial state-of-the-art TFC membranes, considering both pure water permeability and NaCl rejection.

Type of commercial NF membranes	Pure Water Permeability (LMH/Bar)	Salt rejection (NaCl) 2000 ppm (%)	Reference
NF3	~12.5	~15	[13]
Duracid	~0.5	~70	[13]
NF 90	~0.57	~60	[14]
NF 270	~0.52	~48	[14]
PES TEC	~8	~28	[15]
PES TFC	~12.7	~61	This study
RG PVC TFC	~14.5	~57	This study
Upcycled PVC TFC	~17.2	~46	This study

S9. References.

[1] P.A. Vinodhini, P.N. Sudha, Removal of heavy metal chromium from tannery effluent using ultrafiltration membrane, Textiles and Clothing Sustainability, 2 (2016) 5.
[2] X. Shen, T. Xie, J. Wang, P. Liu, F. Wang, An anti-fouling poly(vinylidene fluoride) hybrid membrane blended with functionalized ZrO2 nanoparticles for efficient oil/water separation, RSC Advances, 7 (2017) 5262-5271.
[3] S. Surawanvijit, A. Rahardianto, Y. Cohen, An Integrated approach for characterization of polyamide reverse osmosis membrane degradation due to exposure to free chlorine, Journal of Membrane Science, 510 (2016) 164-173.

[4] P. Karami, B. Khorshidi, J.B.P. Soares, M. Sadrzadeh, Fabrication of Highly Permeable and Thermally Stable Reverse Osmosis Thin Film Composite Polyamide Membranes, ACS Applied Materials & Interfaces, 12 (2020) 2916-2925.
[5] X. Tan, D. Rodrigue, A Review on Porous Polymeric Membrane Preparation. Part I: Production Techniques with Polysulfone and Poly (Vinylidene Fluoride), Polymers (Basel), 11 (2019).
[6] S. Kasemset, L. Wang, Z. He, D.J. Miller, A. Kirschner, B.D. Freeman, M.M. Sharma, Influence of polydopamine deposition conditions on hydraulic permeability, sieving coefficients, pore size and pore size distribution for a polysulfone ultrafiltration membrane, Journal of Membrane Science, 522 (2017) 100-115.
[7] C. Combe, E. Molis, P. Lucas, R. Riley, M. Clark, The effect of CA membrane properties on adsorptive fouling by humic acid, Journal of Membrane Science, 154 (1999) 73-87.
[8] X. Dong, A. Al-Jumaily, I.C. Escobar, Investigation of the Use of a Bio-Derived Solvent for Non-Solvent-Induced Phase Separation (NIPS) Fabrication of Polysulfone Membranes, Membranes, 8 (2018) 23.
[9] S. De, M. Mondal, Characterization and antifouling properties of polyethylene glycol added PAN-CAP blend membrane, RSC Adv., 5 (2015).
[10] M. Sadrzadeh, S. Bhattacharjee, Rational design of phase inversion membranes by tailoring thermodynamics and kinetics of casting solution using polymer additives, Journal of Membrane Science, 441 (2013) 31-44.
[11] C. Boo, Y. Wang, I. Zucker, Y. Choo, C.O. Osuji, M. Elimelech, High Performance Nanofiltration Membrane for Effective Removal of Perfluoroalkyl Substances at High Water Recovery, Environmental Science & Technology, 52 (2018) 7279-7288.
[12] D. Chen, J.R. Werber, X. Zhao, M. Elimelech, A facile method to quantify the carboxyl group areal density in the active layer of polyamide thin-film composite membranes, Journal of Membrane Science, 534 (2017) 100-108.
[13] E.Q. Lim, M.Q. Seah, W.J. Lau, H. Hasbullah, P.S. Goh, A.F. Ismail, D. Emadzadeh, Evaluation of Surface Properties and Separation Performance of NF and RO Membranes for Phthalates Removal, Membranes, 13 (2023) 413.
[14] M.B.M. Ang, Y.-L. Wu, M.-Y. Chu, P.-H. Wu, Y.-H. Chiao, J. Millare, S.-H. Huang, H.-A. Tsai, k.-r. Lee, Nanofiltration Membranes Formed through Interfacial Polymerization Involving Cycloalkane Amine Monomer and Trimesoyl Chloride Showing Some Tolerance to Chlorine during Dye Desalination, Membranes, 12 (2022) 333.
[15] X. Zhang, J. Tian, R. Xu, X. Cheng, X. Zhu, C.Y. Loh, K. Fu, R. Zhang, D. Wu, H. Ren, M. Xie, In Situ Chemical Modification with Zwitterionic Copolymers of Nanofiltration Membranes: Cure for the Trade-Off between Filtration and Antifouling Performance, ACS Applied Materials & Interfaces, 14 (2022) 28842-28853.